



**NATIONAL CENTRE FOR
GROUNDWATER
RESEARCH AND TRAINING**

Simulating the groundwater flow dynamics of fault zones

MODFLOW Un-Structured Grid: A comparison of methods for representing fault properties and a regional implementation

McCallum J., Simmons C., Mallants D., Batelaan O.

2018

This report was commissioned by the Department of the Environment and Energy.

Authorship

James McCallum ^{1,2}, Craig Simmons ^{1,2}, Dirk Mallants ³ and Okke Batelaan ^{1,2}

Affiliation

- 1 – School of the Environment, Flinders University
- 2 – National Centre for Groundwater Research and Training
- 3 – CSIRO Land and Water

Acknowledgement

The authors would like to acknowledge the Department of the Environment and Energy for funding the project “Research to improve treatment of faults and aquitards in Australian regional groundwater models to improve assessment of impacts of CSG extraction”. The Authors equally wish to thank Julian Strand for his contribution to the methodology on non-neighbour connection, conceptualisation of the up-fault model and provision of the regional geology model. The report was subject to internal peer review processes during its development and benefitted from reviews undertaken by Rodd Dan (Department of the Environment and Energy), Scott Lawson (Department of the Environment and Energy), Dr. Peter Cook (Flinders University) and Dr. Saskia Noorduijn (Flinders University).



EXECUTIVE SUMMARY

Faults play an important role in flow and transport in regional groundwater systems. For this reason, the inclusion of faults in regional groundwater models is important when considering the impacts of coal seam gas extraction. Faulting modifies groundwater systems in two ways. Firstly, faulting causes discontinuities in layers at faults (juxtaposition). Depending on the permeability of the layers on adjacent sides of the fault, the juxtaposition effects (which is only related to layer geometry) can either keep fluxes the same, change their direction or decrease them. Secondly, a number of processes that modify rocks both during and after faulting may act to enhance or reduce permeability in the region of the fault itself. The modifications to permeability represent a range of behaviours at and around fault planes that can broadly be described as: a barrier – where faults act to reduce the flux, a conduit – where faults act to allow across or up fault fluxes, or a conduit/barrier – where the flux is enhanced parallel to the fault and reduced perpendicular to the fault. It is therefore important for groundwater modelling to represent modifications to layering and the conduit and/or barrier behaviour of faults.

The most recent version of MODFLOW, MODFLOW Un-Structured Grid offers great flexibility for grid development (i.e. inclusion of geological structures such as faults) as it allows the user to define connections between different layers and modify permeability properties directly. Within the context of user defined connection properties, a number of methods exist for the inclusion of modified fault properties. These methods can account for modification to cross-fault, up-fault and in some cases along-fault flow terms. We tested a number of different representations of fault property modification techniques. We determined that for the barrier scenario, all of the methods showed excellent agreement. This suggests that if a fault can be identified as a barrier to flow, the use of a lower-numerical cost solution is appropriate. For scenarios where faults had conduit or conduit/barrier behaviour, poor agreement was observed between the methods. This most likely related to the difference in conceptualisation, as only some methods accounted for along-fault flow (most assume conduit flow as up-fault flow). Additionally, not all of the proposed methods could be executed in current MODFLOW Un-Structured Grid solvers, limiting their applicability.

We further implemented a technique that represented fault properties in a regional scale model based on the structure of the Gloucester basin in New South Wales. We were able to obtain model convergence on a large grid and tested three conceptualisations of fault permeability modification. Our results suggested that for the system modelled, the barrier and the conduit/barrier method produced very similar results. Both showed that the fault acted as a barrier to the extent of the drawdown occurring during pumping. The conduit conceptualisation had a significantly different outcome, with drawdowns extending past the fault plane. These differences suggest that the conceptualisation of faults is an important factor when predicting the impacts of coal seam gas extraction. Ideally, fieldwork and monitoring should focus on identifying how a fault is behaving at a site of interest. However, in the absence of definite evidence a robust sensitivity analysis should account for the conceptual uncertainty of fault behaviour.

Contents

Executive summary	2
Abbreviations	6
Symbols	7
Glossary	8
1. INTRODUCTION	12
2. PHYSICAL PROPERTIES OF FAULTS.....	12
1.1 Layer Offset.....	12
1.2 Permeability Modification	14
1.2.1 Primary processes	14
1.2.2 Secondary processes.....	16
1.3 Conceptualisation of Fault Zones	16
1.3.1 Generic models	16
1.3.2 Fault property relationships.....	18
2. EXISTING FAULT MODELLING APPROACHES	19
2.1 Discrete Fracture Network Modelling	19
2.2 Continuum Approaches.....	19
2.3 Modified Conductance Approach (Manzocchi method)	20
3. MODFLOW UNSTRUCTURED GRID AND FAULT REPRESENTATION.....	20
3.1 Overview of numerical approach	20
3.2 Numerical implementation of control volume finite difference method	22
3.3 Ghost Node Correction (GNC)	23
4. IMPLEMENTATION OF CROSS-FAULT FLOW	25
4.1 Identification of non-neighbour connections	25
4.2 Cross-Fault Permeability Modification	29
4.2.1 Modified Conductance Approach (Manzocchi method)	29
4.2.2 Continuum approach.....	29
5. IMPLEMENTATION OF UP-FAULT FLOW CONNECTIONS	30
5.1 Modified Conductance (Manzocchi) and vertical conductance	30
5.2 Modified Manzocchi with cross and up-fault connections.....	30
5.3 Continuum approach.....	31
6. METHOD COMPARISON	32
6.1 Governing Equations.....	32
6.2 Local-scale model implementation.....	33
6.3 Results	36
7.1 Model Description	38
7.2 Results	41
8. DISCUSSION.....	47
9. SUMMARY OF PROGRESS	49
10. REFERENCES	50

Figures

Figure 1: The geometric modification of aquifer/aquitard sequences due to faulting.

Figure 2: Numerical Solution of hydraulic heads (m), streamlines (m^2/s) and solute concentration (mole/m^3) in the vicinity of a fault zone for a fault throw of 200 m. Simulations are for the model in which the fault has no permeability modifications (a–c), the modified fault permeability is isotropic (d–f) and the modified fault permeability is anisotropic (g–i). (Bense and Person 2006)

Figure 3: Conceptualisations of fault zone architecture in (a) crystalline (deep) media and (b) unconsolidated (shallow) media, showing fault core (FC), damage zone (DZ), and mixed zone (MZ) (Loveless et al., 2011). Reprinted from Journal of Structural Geology, Volume 33, Issue 11, S. Loveless, V. Bense, J. Turner, Fault architecture and deformation processes within poorly lithified rift sediments, Central Greece, Pages 1554-1568, Copyright (2011), with permission from Elsevier.

Figure 4: Three conceptual models of how fault zones impact fluid flow properties. DZ = damage zone (modified from Bense et al. 2013).

Figure 5: (A) conceptual model of a faulted system and (B) equivalent numerical grid implementation in MODFLOW Un-structured Grid (Panday et al. 2013).

Figure 6: Demonstration of the limitation of the control volume finite difference approach to faulted systems. In the un-faulted system (a), cell centres are connected by a line perpendicular to the cell face. In the faulted system (b), cell centres are not connected by a line perpendicular to the cell face.

Figure 7: Schematic for the ghost node correction scheme in two dimensions. The correction is applied to the blue cell. The connected area between the flat (blue) layer and the sloped (red) layer is defined by the green area. The Green square represents the ghost node.

Figure 8: (a) description of cell edges and centres used for identifying connections. (b) Depiction of the connected area of two cells. (c) Demonstration of how two connected cells are joined through the centre of the connected area. (d) example of the use of ghost nodes to ensure the connection honours the requirements of the control volume finite difference method.

Figure 9: Schematic for identifying connections and the vertices of the 17 unique combinations that can form.

Figure 10: Example of (a) a modified conductance approach and (b) a continuum approach. The continuum approach represents the fault zone explicitly with a cell of dimension dx_f and k_f .

Figure 11: Conceptual model for up-fault flow implementation. (a) Modified vertical conductance (dashed yellow lines) in cells neighbouring the fault. (b) Direct connections (note only connections for the bottom left cell are shown) and (c) the continuum approach where up-fault flow occurs through a series of connected thin 'fault cells'.

Figure 12: Schematic for the modified Manzocchi method with cross and up-fault flow connections.

Figure 13: (a) Conceptual model (Childs et al. 2009) and (b) grid of test model. The grid is a 7 by 12 by 3 cells. The horizontal discretisation is 10 m and the vertical discretisation is 5 m. Part A reprinted from Journal of Structural Geology, Volume 31, Issue 2, C. Childs, T. Manzocchi, J. J. Walsh, C. G. Bonson, A. Nicol, M. P. J. Schöpfer, A geometric model of fault zone and fault rock thickness variations, Pages 117-127, Copyright (2009), with permission from Elsevier.

Figure 14: Permeability models of faults as (a) barrier, (b) conduit and (c) conduit/barrier systems. These conceptual models are taken from Aydin (2000). DZ represents the damage zone and FC represents the fault core. The models here are for a wall rock with a permeability of 1 mD.

Figure 15: An example simulation using the continuum approach and the conduit/barrier conceptualisation of the fault system.

Figure 16: Implementation of the continuum method in MODFLOW Unstructured grid

Figure 17: Model setup with (a) plan view with layer numbers (variability in layer numbers at the surface is due to fault juxtaposition), (b) cross section view of model domain (showing discontinuities created by faulting), and (c) Hydraulic conductivity distribution. Part (a) also shows the location of the cross sections used for head and drawdown results.

Figure 18: Initial head distributions for the three fault conceptualisations. The fault locations are represented by the dashed lines. The location of the transect line is shown in Figure 17.

Figure 19: Drawdowns after 365 days. The location of the transect line is shown in Figure 17.

Figure 20: Layer-averaged drawdown along East-West transect (orthogonal to the faults). The Fault is located at 5000 m.

Figure 21: Vertical head distributions for different fault flow conceptualisations.

Abbreviations

Abbreviation	Description
CVFD	Control volume finite difference
DFN	Discrete fracture network
DZ	Damage zone
FC	Fault core
GNC	Ghost Node Correction
MODFLOW-USG	MODFLOW un-structured grid
SGR	Shale Gouge Ratio

Symbols

Symbol	Short description
A	Area
b	thickness
b_f	fault thickness
C	Centre
CL12	The length between two connected cells
C_{mn}	Conductance between cells m and n
dx	discrete step in the x-direction
dx_f	Discrete distance of a fault
dz	discrete step in the z-direction
FAHL	The area or width of a connection
h_j	A head that contributes to a ghost node
h_m	The head in node m
h_n	the head in node n
IVC	This indicates whether a connection is horizontal (IVC =0) or vertical (IVC=1)
JA	Identifier of Node Connections
k	permeability
k_f	permeability of a fault
K_h	Horizontal hydraulic conductivity
K_{par}	Hydraulic conductivity parallel to a fault
K_{perp}	Hydraulic conductivity perpendicular to a fault
Ksat	The saturated conductivity of a connection
K_v	Vertical hydraulic conductivity
K_x	Hydraulic conductivity in the x-direction
K_z	Hydraulic conductivity in the z-direction
S_s	Specific storage
S_y	Specific yield
α_j	The contribution of head j to a ghost node

Glossary

Term	Description
Alluvium	A sedimentary environment deposited by the movement of water in streams over time.
Along fault flow	Flow occurring immediately parallel to a fault plane.
Anisotropic	Having different physical properties in different directions.
Aquifer	A porous or fractured media where water is easily transmitted due to a relatively high permeability.
Aquitard	A saturated body of rock or stratum of sediment that is less permeable than an aquifer and incapable of transmitting useful quantities of water. Aquitards often form a confining layer over an artesian aquifer.
Breccia	A rock composed of broken fragments of rock or minerals embedded in a fine-grained matrix.
Brecciation	The process of high density faulting resulting in the formation of breccia.
Cataclasis	The process whereby rock fragments are crushed to fine grains with intergranular sliding and rotation.
Cementation	The process whereby rocks become consolidated through chemical precipitation resulting in a reduction in porosity.
Clay smear	The smearing of clays occurring due to the movement of rock during faulting.
Coal seam	A coal seam is a single layer or bed of coal (sedimentary rock).
Coal seam gas	A form of natural gas (generally 95 to 97% methane, CH ₄) typically extracted from permeable coal seams at depths of 300 to 1000 m. Also called coal seam methane (CSM) or coalbed methane (CBM).
Conductance	A term that contains all components of Darcy's law except the hydraulic head terms.
Confined aquifer	An aquifer that is isolated from the atmosphere by an aquitard or aquiclude. Pressure in confined aquifers is generally greater than atmospheric pressure.
Consolidation	The removal of pore-space due to increased overburden or lateral stress.
Continuum modelling approach	The inclusion of the physical characteristics of fault zones as zones in groundwater flow models.
Control Volume Finite Difference	A numerical method for solving the groundwater flow equation.
Cross fault flow	Flow occurring perpendicular to a fault plane.

Damage zone	The damage zone is the area where the rock is modified, however the stress exerted is less than at the fault.
Darcy's Law	The governing equation for groundwater flow. It states that flow is proportional to hydraulic conductivity, hydraulic gradient and cross sectional flow area.
Discrete fracture modelling	A modelling approach where the fluid flow in individual fractures is simulated.
Dissolution	A chemical process where minerals are dissolved in water.
Empirical modelling approach	The inclusion of fault properties in groundwater flow models by modifying existing model conductance's.
Fault	A discontinuity on geological units occurring as a result of shear stress.
Fault core	The centre of the fault where modification has occurred due to high levels of stress and movement.
Fault throw	The vertical component of dip separation.
Fault zone	The Fault zone refers to the zone perpendicular to a fault where modification to the original rock structure is observed. It includes the fault core and damage zone.
Fracture	A crack occurring in a consolidated rock due to stress and shear.
Fracturing	The process by which fractures are created.
Gouge	Unconsolidated tectonite (a rock formed by tectonic forces) with a very small grain size.
Groundwater	Water occurring naturally below ground level (whether in an aquifer or other low-permeability material), or water occurring at a place below ground that has been pumped, diverted or released to that place for storage. This does not include water held in underground tanks, pipes or other works.
Hydraulic barrier	An object that restricts fluid flow and pressure propagation.
Hydraulic conductivity	The amount of water transmitted by a porous media for a unit area and a unit hydraulic gradient.
Hydraulic conduit	An object that locally enhances fluid flow and pressure propagation.
Hydraulic connection	A pathway between two units by which water can be transmitted.
Hydraulic gradient	The change in hydraulic head between different locations within or between aquifers or other formations, as indicated by bores constructed in those formations.
Impermeable	This is used to refer to a unit with a low permeability.
Milli Darcy (mD)	Measurement unit for permeability.
MODFLOW	An Industry standard groundwater model developed by the US Geological Survey.

MODFLOW Un-structured Grid	A version of MODFLOW that simulates groundwater flow on irregular grids.
Node	A discrete point or volume for which a head is calculated for using numerical solution of Darcy's Law.
Numerical groundwater model	A numerical groundwater model divides space and/or time into discrete pieces. Features of the governing equations and boundary conditions (e.g. aquifer geometry, hydrogeological properties, pumping rates or sources of solute) can be specified as varying over space and time. This enables more complex, and potentially more realistic, representation of a groundwater system than could be achieved with an analytical model. Numerical models are usually solved by a computer and are usually more computationally demanding than analytical models.
Particle size	A measure of the size of particles that make up unconsolidated or consolidated rocks.
Particulate flow	Particulate flow refers to the movement of unconsolidated grains during faulting. This can also include particles generated from solid rock during faulting.
Permeability	The measure of the ability of a rock, soil or sediment to yield or transmit a fluid. The magnitude of permeability depends largely on the porosity and the interconnectivity of pores and spaces in the ground.
Permeable	This is used to refer to a unit with a high permeability.
Precipitation	The process whereby minerals at saturation in water precipitate as solids.
Recharge	Groundwater recharge is the process whereby surface water (such as from rainfall runoff) percolates through the ground to the water table.
Regional groundwater model	A model of groundwater for a regional area.
Seal	The truncation of an aquifer unit due to a low permeability unit of a low permeability fault zone, potentially resulting in retention and accumulation of hydrocarbons.
Specific storage	The volume of water needed to reduce the head in a unit thickness of confined aquifer.
Specific yield	The volume of water required for a unit area of unconfined aquifer to reduce the hydraulic head by 1 unit.
Throw	The vertical component of dip separation of a fault.
Transmissivity	A measure of the ability of saturated aquifers to transmit water. Taken as the Hydraulic conductivity times the saturated thickness.
Up fault flow	Flow occurring immediately parallel to a fault plane, in a vertical or near – vertical direction.

Unconsolidated

This refers to porous media that has not undergone processes of compaction and cementation where the grains remain separate.

1. INTRODUCTION

Regional scale groundwater models are commonly used to investigate potential effects of coal seam gas and coal mining developments. A key element of such investigations is to develop and parameterise regional-scale groundwater models that accurately represent the properties of the rock framework and effects of mining and coal seam gas development, including groundwater depressurisation and its potential propagation via faults to water supply aquifers and streams. In a recent review Underschultz et al. (2018) provide a framework that can be used to guide research into appropriate methodologies and procedures of fault zone parameterisation and representation in regional-scale groundwater models. The review considers methodologies for estimating the properties of faults and how these can be represented in regional-scale groundwater models.

Turnadge et al., (2018) reviewed fault architecture, distributions and processes that alter fault zone permeability; they also reviewed the current methodologies for implementation of faults in groundwater models. These authors identified that representation of faults in groundwater flow models for coal seam gas-related impact assessments in Australia is rare: only two out of ten groundwater impact studies that had reported inclusion of faults, did so by modifying the conductance between neighbouring model cells in order to represent barriers or conduits to flow. This approach cannot be used to represent complex anisotropic fault conceptualisations (e.g., cross-fault barrier/along-fault conduit structure); also, fracture zones surrounding the fault core were not simulated in any of the models. Turnadge et al. (2018) conclude that considerable improvement is needed to better represent fault geometry and flow properties in groundwater flow models.

2. PHYSICAL PROPERTIES OF FAULTS

To best understand the requirements of fault representation in models we must first examine the physical properties of faults and how they impact groundwater flow. This section briefly outlines the physical properties of faults which need to be considered, particularly in reference to fault permeability, for their inclusion in groundwater flow models. Additional information can be found in a review of fault zone implications for groundwater flow by Bense et al. (2013).

1.1 Layer Offset

The first physical aspect of faulting considered here is the offsetting of stratigraphic layers (Figure 1). If layers are deposited in a sedimentary sequence a layered system will form. The layers composed of fine grained sediments will have a low permeability and layers composed of coarse grained sediments will have a high permeability. In the absence of any permeability modifications that occur due to faulting (discussed in Sections 1.2 and 1.3), the connection/ disconnection, due to faulting, of layers with varying permeabilities can result in changes to the fluid flow properties of a system at both small and large scales (Allan, 1989; Matthäi and Roberts, 1996). Typical modifications that occur across a fault are depicted in Figure 1 and can be described as:

1. The disconnection or discontinuity of permeable layers (also called “sealing”) where an aquifer layer is fully off-set across the fault, being juxtaposed an aquitard,
2. A local reduction in the cross-sectional flow area of conductive layers (and therefore transmissivity) can create a relative restriction to flow within an aquifer unit that would not exist

in the absence of faulting. This is where an aquifer is partially off-set across a fault resulting in its juxtaposition with only part of the aquifer on the other side of the fault,

3. The connection of permeable units that would otherwise not exist if faulting had not occurred (enabling continuity or enhancement). This is where an aquifer is fully off-set and juxtaposed a different aquifer with different hydraulic properties.

The implications of these modifications to the stratigraphic build-up and interconnectivity between conductive layers are important. In the case of sealing (example 1. above), if faulting was not considered in a groundwater model, the assumption of an extensive aquifer may lead to poor predictions. For example, drawdown due to pumping may be underestimated as the connected aquifer volume is much smaller when faulting results in compartmentalisation. When the flow area becomes restricted due to partial offset of a conductive layer (example 2. above), despite the partial continuity of the conductive layer still existing, the local reduction in the transmissivity of the aquifer will restrict flow and may result in a build-up of water pressure on the up-gradient side of the fault. In the third case, if faulting were not incorporated in a groundwater model and two conductive layers are assumed to be separated by an aquitard, the potential interaction between the layers will be misrepresented, causing errors in the predictions made. However, if the effects of faulting are accounted for in the model, the hydraulic connection created between the two permeable units will result in hydraulic stresses originating in one layer being transmitted to the connected unit.

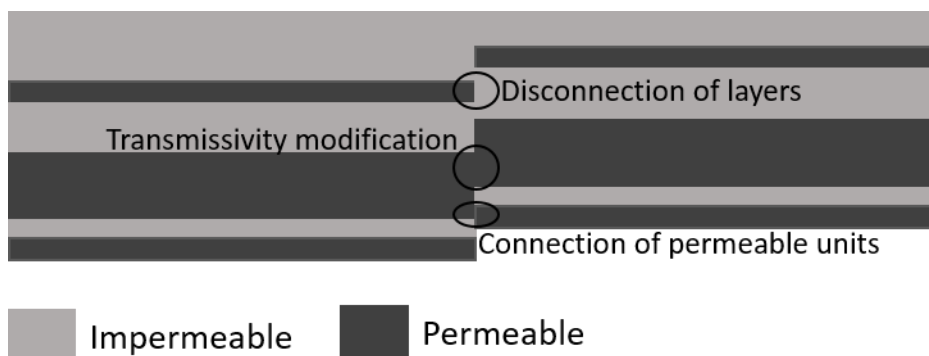


Figure 1: The geometric modification of aquifer/aquitard sequences due to faulting.

The throw (i.e., vertical displacement) of faults and the layer offsets they create are spatially variable. This means that at different points along a fault the connections caused by a fault will vary. This makes the three-dimensional representation of faults important as a two-dimensional representation at a point along a fault may yield a gross simplification of flow paths. In the absence of permeability modifications, the impacts of faults will be to create tortuous flow paths across faults depending on the distribution of high and low permeable units (Figure 2). Modifying the fault hydraulic properties will also modify groundwater flow (and solute transport) as indicated in Figure 2. Clearly under certain circumstances faults will have impacts on hydraulic head, flow path and concentration distributions.

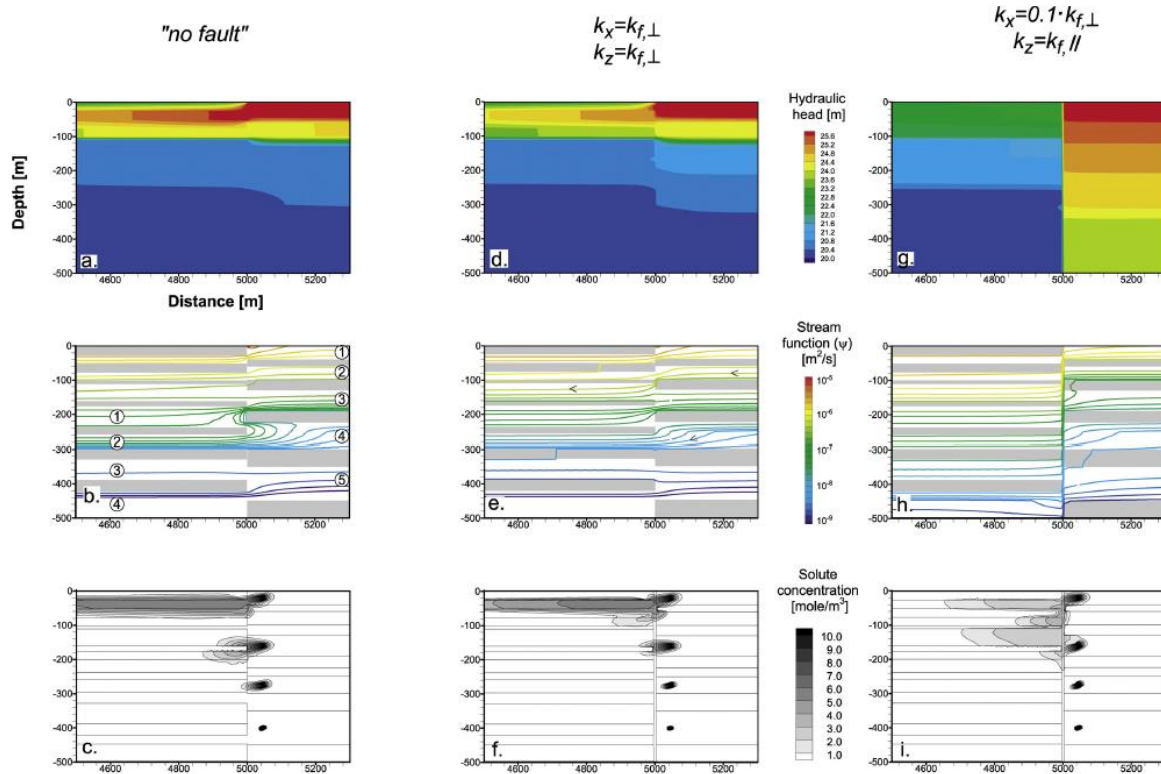


Figure 2: Numerical Solution of hydraulic heads (m), streamlines (m²/s) and solute concentration (mole/m³) in the vicinity of a fault zone for a fault throw of 200 m. Simulations are for the model in which the fault has no permeability modifications (a–c), the modified fault permeability is isotropic (d–f) and the modified fault permeability is anisotropic (g–i). Note ‘no fault’ is an indication of no modification to the properties (Bense and Person 2006)

1.2 Permeability Modification

In addition to the offsetting of layered structures with differing permeability, processes during (primary) and after faulting (secondary) may also act to modify the permeability within fault zones (see discussion in section 1.2.1 and 1.2.2). The total width of a fault zone is made up of two components – the fault core (FC) and the damage zone (DZ) (Bense et al., 2013; Loveless et al., 2011). The fault core represents the location of the greatest strain and displacement. The damage zone represents the area adjacent to the fault core where a smaller amount of strain is dispersed. The permeability of these two zones will be dependent on a number of processes. We will split these processes into primary and secondary processes.

1.2.1 Primary processes

In unconsolidated rocks, the process of particulate flow may act to enhance or reduce permeability (Du Bernard et al., 2002). The stress occurring during faulting first acts to form dilation bands where grains initially move apart. Once the grains have moved apart, the dilation bands become shear bands. In the shear bands, individual grains move past each other in a process called particulate flow. During this movement, individual grains will rotate and align differently. This will lead to some modification of permeability. This process may result in the grains aligning adjacent to the direction of the fault displacement. The permeability changes will be dependent on the distribution and shape of the grains. For example, if grain morphology is angular and alignment occurs in the direction of the fault

displacement, an increase in permeability may occur parallel to the fault displacement whilst a reduction occurs perpendicular to the fault displacement. In coarse grain sediments (i.e. sands and gravels) particulate flow generally results in an increase in permeability (Bense et al., 2003; Du Bernard et al., 2002; Exner and Grasemann, 2010) however, in fault zones with a mix of sediments, the process can result in a reduction in permeability (Heynekamp et al., 1999; Rawling and Goodwin, 2006). This can arise due to the smearing of clays.

Another primary process that modifies the permeability of fault zones, in consolidated/hard rock, is the fracturing that occurs in damage zones immediately adjacent to the fault core. This fracturing (strain) occurs in consolidated rocks due to the stress imposed on the rocks. The permeability change will be dependent on the fracture density and connectivity (Bour and Davy, 1997) and on fracture aperture (Long et al., 1982). The general outcome of this process is to increase the permeability in the damage zone (Bense et al., 2013). The increase in permeability due to fracturing has been observed in a number of different settings (e. g. Martel, 1990; Eichhubl et al., 2009; Balsamo et al., 2010).

Fault cores in crystalline rock occur as relatively narrow, localized zones containing modified media including breccias and cataclastic material (Figure 3, Loveless et al. 2011). The process of brecciation is an extension of fracturing. In this process the fractures in the rock associated with faulting are filled angular rock fragments in a matrix of fine grained material. This produces a rock called breccia. Breccia can result in an increased permeability of the fault core in the absence of cementation and also occurs in the damage zone (Bense et al., 2013). Examples of increases in permeability due to brecciation are included within Caine et al. (2010) and Roberts and Stewart (1994). The invasion of fine sediments into fractures or cementation of the structure by diagenetic processes may also act to reduce the permeability of the damage zone (Benedicto et al., 2008; Gibson, 1998; Schulz and Evans, 2000). Hence this process can act to either increase or reduce the permeability of fault zones.

The process of cataclasis occurs as the result of the fracturing of the rock in the core and damage zone which results in rock fragmentation. Continued movement crushes the broken fragments to finer grain size causing smearing and grain alignment. The result of this process is a reduction in permeability (Bense et al., 2013). The process of cataclasis can also result in anisotropy and spatial variability in fault zone permeability (Sigda et al., 1999). The reduction in permeability due to cataclasis has been demonstrated in a number of studies (Sigda and Wilson, 2003; Sigda et al., 1999; Wilson et al., 2003).

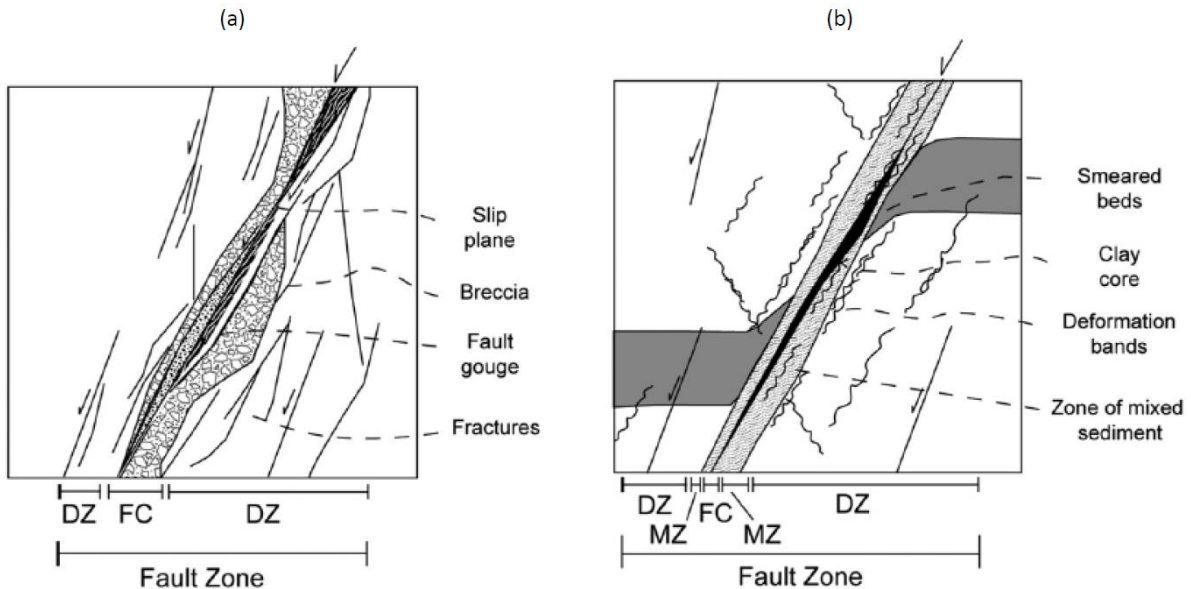


Figure 3: Conceptualisations of fault zone architecture in (a) crystalline (deep) media and (b) unconsolidated (shallow) media, showing fault core (FC), damage zone (DZ), and mixed zone (MZ) (Loveless et al., 2011). Reprinted from Journal of Structural Geology, Volume 33, Issue 11, S. Loveless, V. Bense, J. Turner, Fault architecture and deformation processes within poorly lithified rift sediments, Central Greece, Pages 1554-1568, Copyright (2011), with permission from Elsevier.

1.2.2 Secondary processes

After the formation of faults, a number of processes can impact the permeability of the fault core and damage zone. One of these is geochemical reactions. If fractures are opened during faulting, fluid flow may occur. The fluid may have originated in a different part of the aquifer (or basin) resulting in non-equilibrium and thus chemical reactions. The exposure of this fluid to new pressure and temperature conditions as it migrates may alter the conditions of saturation of chemical species, resulting in the precipitation of minerals (e.g. iron oxides) within fractures (Bense et al., 2013). This cementation of the pore space will result in a reduction in the aperture and hence the permeability of the fractures. Conversely, water that is under-saturated with respect to the rock minerals may cause dissolution of the matrix (e.g. carbonates). This will increase the aperture of fracture and increase the permeability of fault zones (Bense et al., 2013).

Additional secondary processes include sediment filling of fractured zones, compaction and cementation of sediments in and around the fault zone, and the effect of regional stress on fracture apertures (Bense et al., 2013). These processes act to alter the permeability of fault zones over time.

1.3 Conceptualisation of Fault Zones

1.3.1 Generic models

A number of generic models exist to describe the permeability modification of faults. Caine et al. (1996) defined the behaviour of faults as a range between conduit and barrier behaviour assuming that fault zones were a combination of a fault core and surrounding damage zone that can both vary in permeability. The authors used the ratio of the damage zone width to the total fault width to classify the fault as acting as a barrier or conduit to groundwater flow. Areas where a well-established core is

present and where a damage zone is minor or absent can be described as barriers to flow. Areas with a poorly established or non-existent core and a well-established damage zone can be classified as a localised conduit (small ratio of damage zone to total fault width) or a distributed conduit (high ratio of damage zones). Fault zones with a well-established core and damage zone could potentially act as conduit-barrier systems, where the increased permeability of the damage zone creates a conduit to flow parallel to the fault plane, whilst the fault core creates a barrier to cross-fault flow. The model is a simple way to describe the fault behaviour (conduit/barrier) based on the relative widths of the fault core and damage zone.

Aydin (2000) proposed a similar conceptualisation of fluid flow in faults. The author presented three models. Two models comprised a low permeability fault core acting as a barrier, one with a high permeability damage zone and the other without. The third model represented a fault with enhanced permeability due to brecciation. Although this model is slightly different, these three models represent faults as either conduits, barriers or conduit-barrier systems. The main difference between this conceptualisation and that of Caine et al. (1996) is a mechanism for the fault core to behave as a conduit.

Rawling et al. (2001) extended the conceptualisation of faults to unconsolidated sediments. The model included a clay core of low permeability flanked by mixed zones. Depending on the type of aquifer sediments distributed at a fault, the mixed zone may act to either enhance or decrease the permeability of the surrounding sediments. For example, in a clay-sand sequence the mixed zone would be of greater permeability than the clay layer but smaller than the sand layer. These behaviours still fall within the conduit-barrier framework but represent different mechanisms than the previous models of consolidated sediments.

The main outcome of this review is that faults can broadly exhibit three behaviours in a fluid flow context (Fig. 4). These behaviours are:

1. A barrier to both along- and across-fault flow
2. A conduit to both along- and across-fault flow
3. A conduit to along-fault flow and a barrier to across-fault flow

It is therefore important that each of these scenarios is tested in the subsequent numerical analysis.

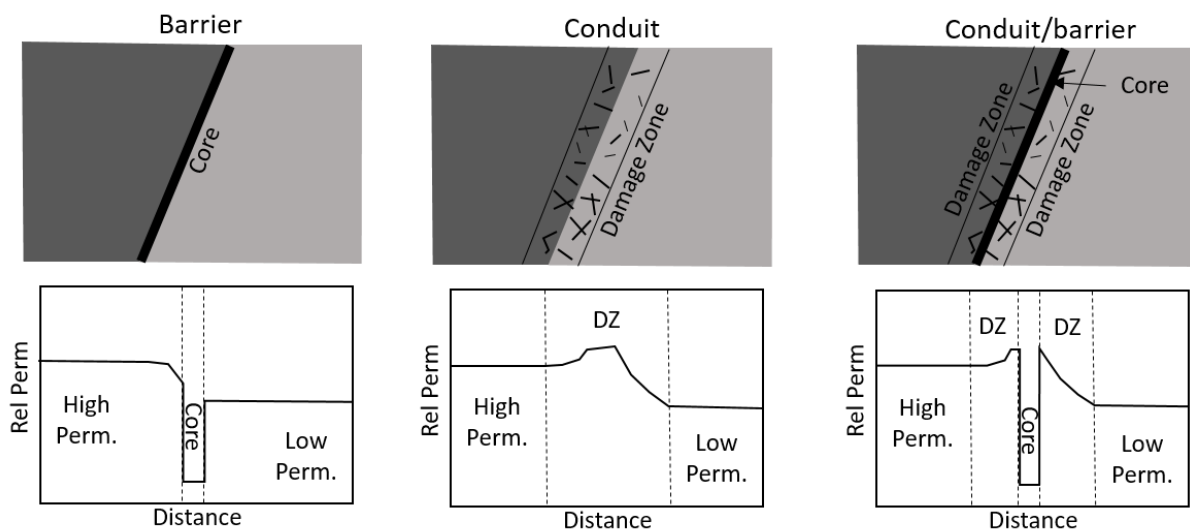


Figure 4: Three conceptual models of how fault zones impact fluid flow properties. DZ = damage zone (modified from Bense et al. 2013).

1.3.2 Fault property relationships

Ideally, to represent the faults within the context of the conceptual conduit-barrier system, details of the physical characteristics of the fault zones need to be represented. This includes the widths and permeabilities of the fault core and the damage zone. The relationship between the width of faults and throw (displacement) of faults is well known (Childs et al., 2009; Gillespie et al., 1993; Walsh and Watterson, 1988). The relationship is often used to estimate fault throw from observations of fault thickness at outcrops (Bense et al., 2013). However, there is some ambiguity around the definitions of fault widths used in some comparison studies. The study of Childs et al. (2009) disaggregated the data into different components of fault thickness, which included the fault core width (referred to by the authors as fault rock) and the damage zone width. The authors found that the fault core to throw followed a relationship of 50:1, meaning the width of the fault core is 0.02 of the throw of the fault. This relationship was found to vary by up to 2.5 orders of magnitude for any given fault throw. The authors found that the damage zone – fault throw relationship was not as well defined.

The permeability of fault rocks is difficult to establish. One of the methods used is the shale gouge ratio (SGR) (Childs et al., 2007; Manzocchi et al., 1999). The SGR is defined as the proportion of clay minerals that have passed a particular point in a fault. The method assumes that the SGR is equivalent to the shale or clay content of the fault zone. This requires some understanding of the rock content around the fault. The SGR is then related to permeability. This method accounts for the permeability of the fault core and does not consider the impacts of the damage zone.

2. EXISTING FAULT MODELLING APPROACHES

The existing fault modelling techniques can be broadly described as discrete fracture modelling, continuum and empirical techniques (Bense et al., 2013). In this section we will give a brief overview of each technique.

2.1 Discrete Fracture Network Modelling

Discrete fracture network (DFN) modelling involves the explicit simulation of fracture networks, for example by using stochastic realisations featuring simplified geometries. In small-scale simulations, typical of a flow domain that includes a single or a few neighbouring faults, faults may be represented as discrete fracture networks, where flow occurs through the fractures formed by the stress and strain regime that led to faulting. Such fractures allow us to conceptualise flow through connected fractures embedded in an otherwise impermeable matrix. The level of detail regarding spatial discretisation and hydraulic property variability required for such simulations far exceeds what is computationally feasible in large-scale regional groundwater flow applications. As such, these models are restricted to the scale of a few 10's to 100's of metres (Bense et al., 2013), although examples exist where DFN approaches have been applied to large-scale systems, including nuclear waste disposal (Herbert, 1996), multiphase flow (Kim and Deo, 2000) and gas flow (Basquet et al., 2003). Although these types of models are difficult to implement as they require determination of fracture network characteristics (e.g. fracture orientation, connectivity, aperture), they may be used to estimate bulk fault zone properties using upscaled approaches (e.g. Fairley, 2009). Due to the data and computational restrictions of this approach, this study will primarily focus on the inclusion of bulk fault zone properties in regional flow models derived through other means. However, the relationship between discrete fracture network models and bulk fault zone properties is an interesting and active area of research (Turnadge et al. 2018), with potential applications to represent explicitly or through some form of upscaling the damage zone at either side of a fault core. Dershowitz et al. (1999), for instance, represented fault damage zones by fracture sets that were generated stochastically using the FRACMAN simulator.

2.2 Continuum Approaches

For larger regional scale applications, continuum approaches can be used to simulate the role of faults (Bense et al., 2013). Here, the bulk properties of faults are represented by equivalent porous media properties. These are generally implemented in conjunction with the offsetting of hydro-stratigraphic units at fault zones. These bulk properties are represented by a fault zone thickness and a fault zone permeability based on integration of one of the fault behaviour models (i.e. combining a damage zone and a fault core). One of the main advantages of this method is that it can be implemented in regional scale models, and the technique allows for the simulation of flow through the faults, allowing for explicit conduit behaviour to be simulated. Some applications may require additional discretisation near the fault zone which may be difficult in structured rectilinear grids, however they may also be able to be represented on an existing grid structure by including some properties of the aquifer/aquitard in the bulk permeability terms. Examples of the implementation of the continuum approach can be found in Leray et al. (2013) and Magri et al. (2010).

2.3 Modified Conductance Approach (Manzocchi method)

In a modification to the continuum approach, the physical properties of faults may be represented by modifying the flow terms of cells connected by faults. For example, if a fault has a low permeability an additional resistance can be added to the flow term between the two cells. The main advantage of this technique is that it effectively maps the fault properties to existing connections. Hence there is no numerical cost for numerical implementation. The method was originally applied by Manzocchi et al. (1999) for cross fault connections in reservoir simulation; it requires quantification of the degree of fault displacement and the shale gouge ratio (see 1.3.2). The latter metric is commonly used to characterise the alteration of fault zone hydraulic properties. In an adaptation of the method, Bense and Person (2006) modified the vertical flow conductance terms of model grid cells adjacent to the fault to simulate up-fault flow properties. The use of transmissivity multipliers has become the industry standard approach to representing faults in reservoir models (Manzochhi et al., 2010).

3. MODFLOW UNSTRUCTURED GRID AND FAULT REPRESENTATION

3.1 Overview of numerical approach

Previous versions of MODFLOW (until the MODFLOW-2005 platform) were based on the implementation of strict layers, rows and columns. The limitation of this rectilinear grid technique was that cells could only be connected to cells in adjacent columns, rows or layers. This meant that the simulation of faulted connections required zoning within layers and partially connected layers could not be implemented.

MODFLOW Unstructured grid (MODFLOW-USG) implements the control volume finite difference (CVFD) technique on unstructured grids (Panday et al., 2013). This effectively allows for the implementation of complex geometries and discontinuous layers (such as those found in faulted systems). The method requires that cells are represented by discrete volumes and connected to adjacent cells. The requirements of accuracy for the method are that:

1. Cell centres are connected perpendicular to the cell face
2. The connection of two cells bisects the face between them

Using MODFLOW–USG allows better representation of faulted systems because of the flexibility in assigning cell connections. Figure 5 provides an example of a faulted system (Fig. 5A) and its discretization using an unstructured grid (Fig. 5B). The grid was constructed by laterally connecting cell 11 to cells 12, 34, and 56. To improve the flux calculation between cells 11 and 56, both of which belong to an aquifer, the so-called ghost-node correction (GNC) package can be used (to be discussed in section 3.3). Ghost nodes would be placed in both cells at the elevation equal to the shared face midpoint.

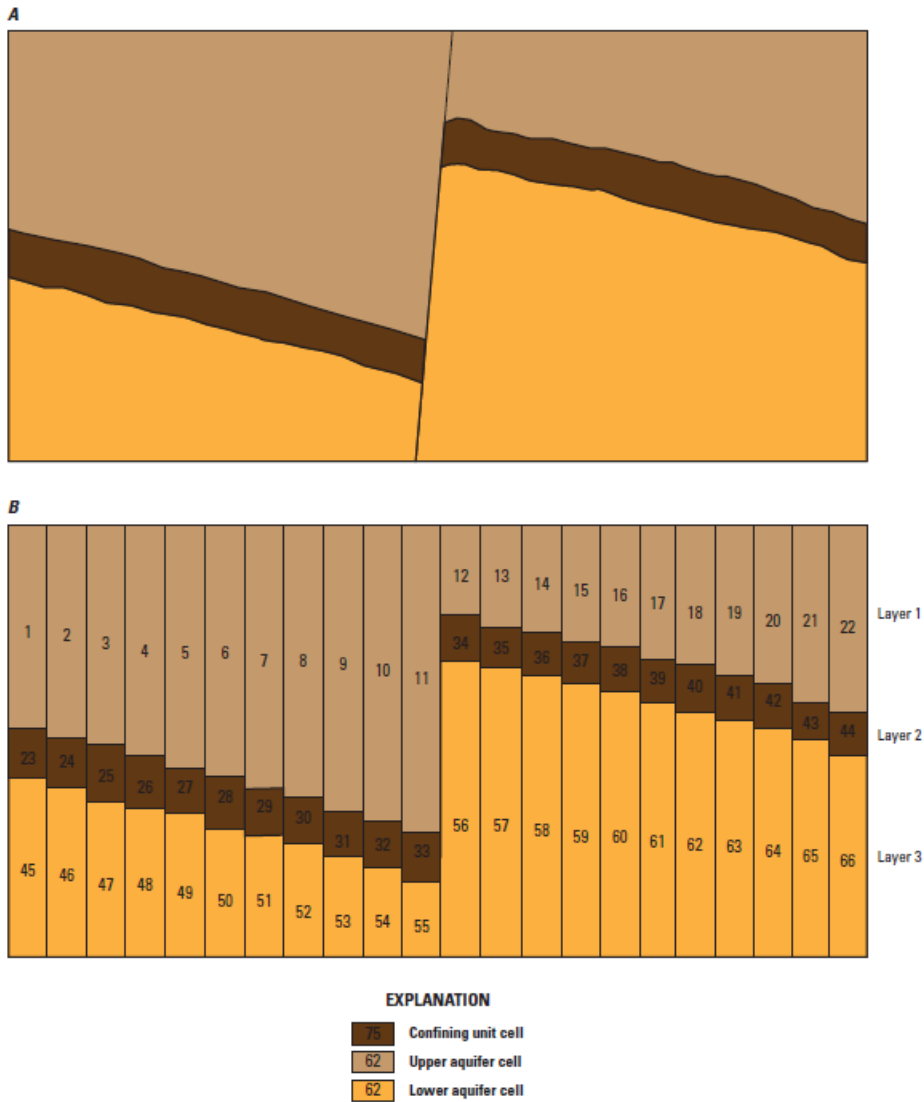


Figure 5: (A) conceptual model of a faulted system and (B) equivalent numerical grid implementation in MODFLOW Un-structured Grid (Panday et al. 2013).

Figure 6 represents the difficulties of meeting the above two requirements in faulted systems. Figure 6a represents an ideal connection, where 2 cells are fully connected and the line between the cells bisects the face of the connection. In Figure 6b, the cells are offset and not fully connected. Additionally, the cell centres do not coincide with a line perpendicular to the cell face. An additional requirement in the MODFLOW-USG implementation is that all cells have flat bottoms and tops which mostly applies to the formulation of horizontal flow connection terms. This is important for unconfined flow, so some of the work we present here only applies to confined aquifers as the connection areas will not vary linearly with head changes when cell bottoms are not flat.

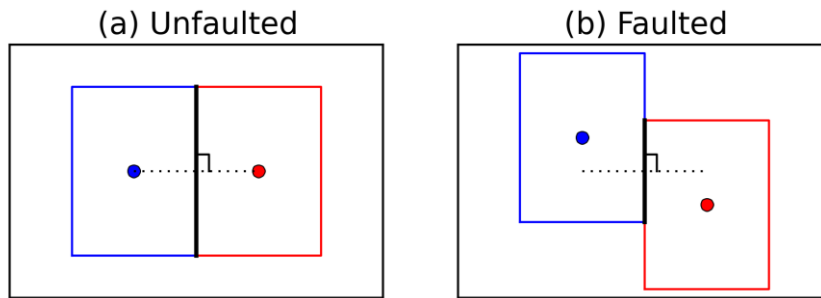


Figure 6: Demonstration of the limitation of the control volume finite difference approach to faulted systems. In the un-faulted system (a), cell centres are connected by a line perpendicular to the cell face. In the faulted system (b), cell centres are not connected by a line perpendicular to the cell face.

To implement the requirements of interface connections when representing faults (Figure 1), ghost nodes may be implemented to meet the criteria. MODFLOW-USG incorporates the use of ghost nodes to meet the criteria of the CVFD method in unstructured grids. Here, the connection between two cells is mapped to multiple nodes. We outline our method for doing this in Section 3.3.

The other main advantage of MODFLOW-USG is that connections can be created between any two cells. Such that hydro-stratigraphic units can be represented as layers but with discontinuities and connections to other layers implemented at faults. This provides great flexibility in the representation of faults zones as horizontal connection between cells in different layers can be implemented. Additionally, vertical connections can be implemented between non-neighbour cells.

3.2 Numerical implementation of control volume finite difference method

The control volume finite difference (CVFD) technique effectively implements Darcy's law and the continuity equation on a finite cell. Each connection in MODFLOW-USG requires the following information for steady-state and transient simulations:

- 1) JA – this is the number of the node that is being connected to
- 2) IVC – this indicates whether a connection is horizontal (IVC =0) or vertical (IVC=1)
- 3) FAHL – this is the area (for vertical connections, L^2) or the width (for horizontal connections, L) for the interface between the connected cells
- 4) CL12 – this is the length of the connection between the cell centre and the interface between the cells (L).
- 5) Ksat – this is the saturated conductivity (for vertical connections and unconfined horizontal connections, LT^{-1}) or transmissivity (for confined horizontal connections, L^2T^{-1}) of the connections.

Additionally, for transient simulations only:

- 6) Ss – the specific storage of the cell (L^{-1})
- 7) Sy – the specific yield of the cell.

It follows that the flow between cells m and n can be described by the equation:

$$Q_{mn} = \frac{Ksat_{mn} \times FAHL_{mn}}{(CL12_{mn} + CL12_{nm})} (h_n - h_m) \quad (1)$$

3.3 Ghost Node Correction (GNC)

Ghost node corrections are essential to ensure the requirements of the CVFD method are met. The term “ghost node” was introduced by Dickinson et al. (2007) to indicate a fictitious node at a location at which the variable of interest (i.e. groundwater head) should be evaluated. Ghost nodes are placed such that the connection between two ghost nodes, or a regular node and a ghost node, bisects the centre of the face at a right angle. These ideal nodes do not necessarily coincide with the cell centres. For this reason, the conductance term associated with the ghost node needs to be mapped to multiple cell centres. The method that we are implementing will primarily be used on horizontally regular (i.e. square) grids with modified layer corrections. The ghost node connections were undertaken using the method of Edwards (1996). This method was chosen as it was easy to implement on the square grids and it accounted for variations in permeability between the cells. A schematic for the ghost node correction scheme is presented in Figure 7.

In multiple dimensions, the head at the ghost node location, h_n , may be obtained as a linear combination of the head values at cell n and of all the adjacent contributing cells h_j as:

$$h_n = \alpha_n h_n + \sum \alpha_j h_j \quad (2)$$

where α_n is the contributing fraction of cell n, Σ the summation over all j contributing cells adjacent to cell n, which are also contributing to the interpolated head value at the ghost node location, and α_j the contributing fraction of each additional contributing cell.

For each non-neighbour connection, the location of the centre of the connection was determined. The method then selected one of the cells above or below and one of the cells adjacent. The two connections were treated separately. In each of the connection cases, the correction was estimated as (Edwards, 1996):

$$\alpha_{1_x} = \frac{dx_n}{dx_1} \frac{K_{x1} dx_1}{\left(\frac{K_{x1}}{dx_1} + \frac{K_{x2}}{dx_2}\right)} + \left(1 - \frac{dx_n}{dx_1}\right)$$

$$\alpha_{1_z} = \frac{dz_n}{dz_1} \frac{K_{z1} dz_1}{\left(\frac{K_{z1}}{dz_1} + \frac{K_{z3}}{dz_3}\right)} + \left(1 - \frac{dz_n}{dz_1}\right)$$

$$\alpha_{2_x} = 1 - \alpha_{1_x}$$

$$\alpha_{3_z} = 1 - \alpha_{1_z}$$

$$\alpha_1 = (\alpha_{1_x} + \alpha_{1_z}) / 2$$

$$\alpha_2 = \alpha_{2_x} / 2$$

$$\alpha_3 = \alpha_{3_z} / 2$$

(3)

where α_n represents the fraction of the conductance mapped to cell n and all other variables are presented in Figure 7. The total contribution was determined by adding the two components for the primary cell together (i.e. the horizontal and vertical components) and dividing that number by two, and dividing the other components of the connections correction by two.

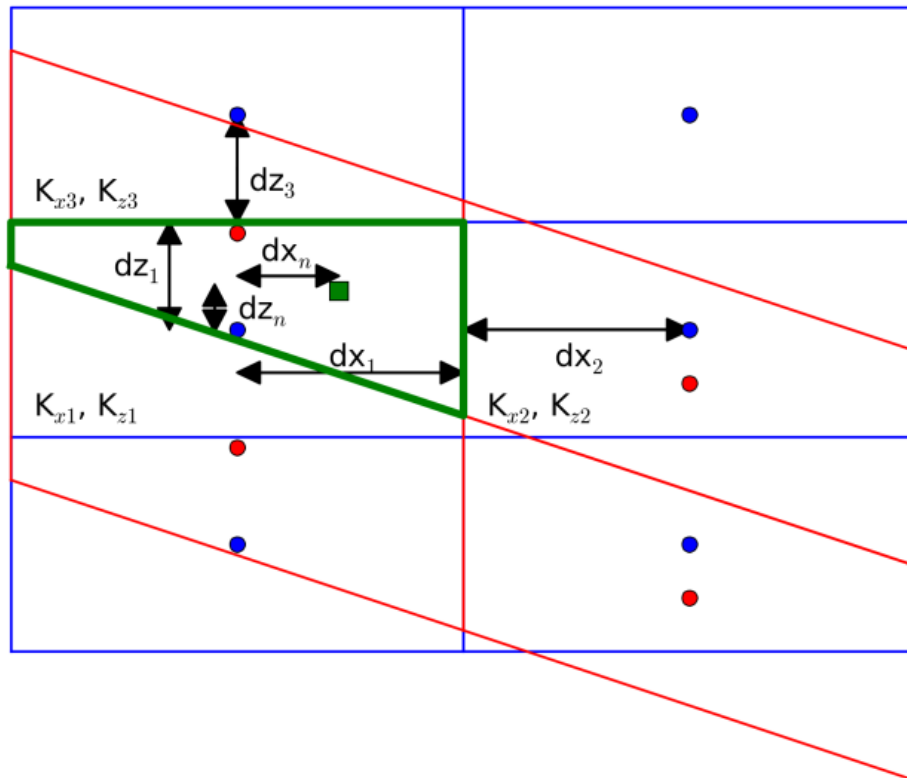


Figure 7: Schematic for the ghost node correction scheme in two dimensions. The correction is applied to the blue cell. The connected area between the flat (blue) layer and the sloped (red) layer is defined by the green area. The Green square represents the ghost node.

4. IMPLEMENTATION OF CROSS-FAULT FLOW

4.1 Identification of non-neighbour connections

The method we present here is implemented on grids where the lateral extents are regular, however faulting has altered the vertical location of hydro-stratigraphic units. We will describe the cells based on their corner points and centres (Figure 8a). In this case the problem can be simplified by using edge configurations to determine the type of connection. If we consider the schematic in Figure 9, adjacent cells can be represented by the two connected faces. For the sake of the example we have called these two faces face A and face B. Each face contains four vertices (Figure 9):

- 0 – the top left vertex
- 1 – the top right vertex
- 2 – the bottom left vertex
- 3 – the bottom right vertex.

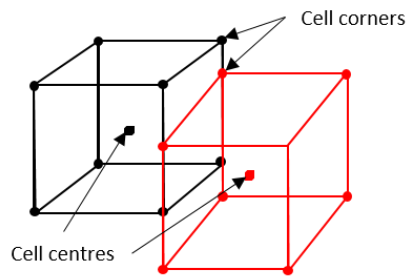
These faces can also be broken down into their edges:

- Top – the line between vertices 0 and 1
- Bottom – the line between vertices 2 and 3
- Left edge – the line between the vertices 0 and 2
- Right edge – the line between vertices 1 and 3.

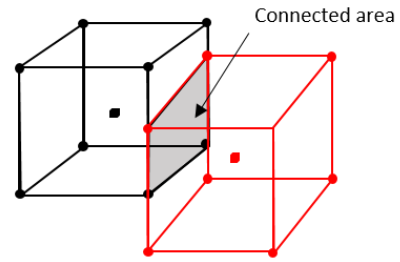
The type of connection can be analysed by examining the elevation of the vertices at the left and right edges. The relative elevation of the vertices of the two faces can be classified into thirteen combinations (Figure 9).

The connected area between two cells (Figure 8b) can also be described by a series of vertices. The vertices can be formed by the corners of either face or the intersection of the bottom or top of a face. The 13 edge combinations produce a total of 17 unique combinations of face connection areas (Figure 9). The edge configurations arising from these cell types are presented in Table 1.

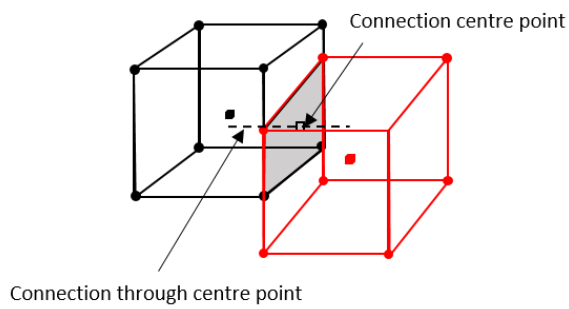
(a) Cell geometry



(b) Identified overlap



(c) Implemented connection



(d) Ghost node implementation

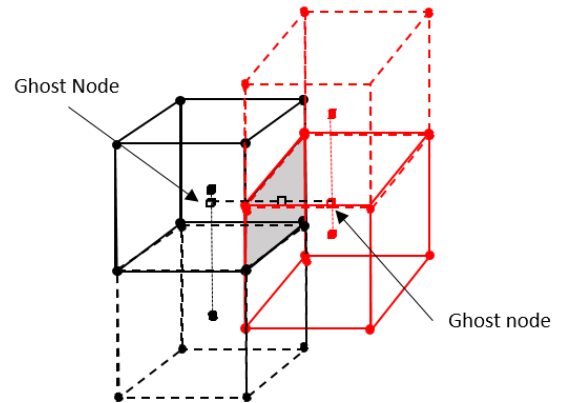


Figure 8: (a) description of cell edges and centres used for identifying connections. (b) Depiction of the connected area of two cells. (c) Demonstration of how two connected cells are joined through the centre of the connected area. (d) example of the use of ghost nodes to ensure the connection honours the requirements of the control volume finite difference method.

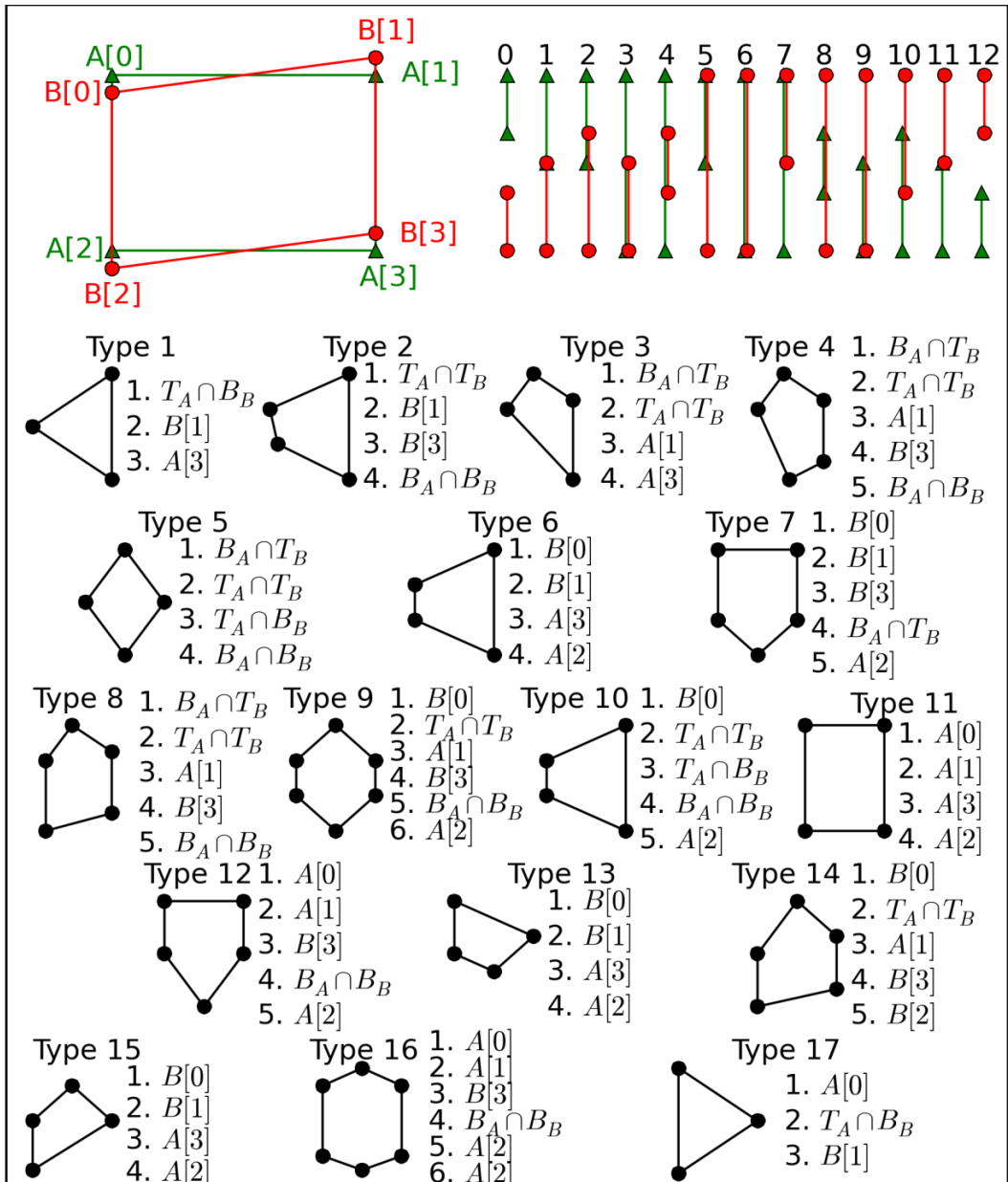


Figure 9: Schematic for identifying connections and the vertices of the 17 unique combinations that can form.

Table 1: Types of connection (Figure 9) dependent on the right and left edge configurations. "0" represents no connected area and "-" represents the reversal of "A" and "B" in the connection type.

		Right Edge Type												
		0	1	2	3	4	5	6	7	8	9	10	11	12
Left Edge Type	0	0	0	1	1	2	1	1	2	3	3	4	5	5
	1	0	0	1	1	2	1	1	2	3	3	4	5	5
	2	-17	-17	6	6	7	6	6	7	8	8	9	10	10
	3	-17	-17	6	6	-11	6	6	-11	8	8	14	15	15
	4	-13	-13	-12	-11	-11	-12	-11	-11	16	14	14	15	15
	5	-17	-17	6	6	7	6	6	7	11	11	12	13	13
	6	-17	-17	6	-11	-11	11	11	-11	11	11	-6	17	17
	7	-13	-13	-12	-11	-11	-7	-6	-11	-7	-6	-6	17	19
	8	-15	-15	-14	-14	-16	11	11	12	11	11	12	13	13
	9	-15	-15	-14	-8	-8	11	-6	-6	11	11	-6	17	17
	10	-10	-10	-9	-8	-8	-7	-6	-6	-7	-6	-6	17	17
	11	-5	-5	-4	-3	-3	-2	-1	-1	-2	-1	-1	0	0
12	-5	-5	-4	-3	-3	-2	-1	-1	-2	-1	-1	0	0	

The important aspect is to calculate the area of the connection and the centre of the connection (Figure 8b and 8c). These two quantities are required to implement the control volume finite difference method. The simplest way to do this is to break the connected areas down into a number of triangles. The calculation for the area and the centre is very simple for triangles and the overall estimates can be made using the following equations:

$$A_T = \sum_{n=1}^{nt} A_n \quad (4)$$

and:

$$C_T = \frac{1}{A_T} \sum_{n=1}^{nt} A_n C_n \quad (5)$$

where A_T is the total area, A_n is the area of the n th triangle, nt is the total number of triangles, C_T is the centre of the total area and C_n is the centre of the individual triangle. The area can be used directly in the MODFLOW-USG code as the variable *FAHL* for vertical connections or incorporated in to the conductance term for horizontal connections. The centre is used to implement the ghost node corrections to ensure that the connections bisect and are perpendicular to the faces (Figure 8d). The remaining components of the method require the definition of the fault properties, namely the thickness and the permeability. The next section examines how these two aspects fit together.

4.2 Cross-Fault Permeability Modification

4.2.1 Modified Conductance Approach (Manzocchi method)

The method of Manzocchi et al. (1999) proposed the representation of faults through a modified conductance approach. Figure 10a presents a schematic to illustrate this method. In this case, the fault is not explicitly modelled, however the effects of the fault permeability (k_f) and the fault zone thickness (dx_f) are accounted for in a conductance term. The permeability of the connection between cell 1 and cell 2 in Figure 10a results from the harmonic mean (k_{12}):

$$k_{12} = \frac{dx_1 + dx_f + dx_2}{\frac{dx_1}{k_1} + \frac{dx_f}{k_f} + \frac{dx_2}{k_2}} \quad (6)$$

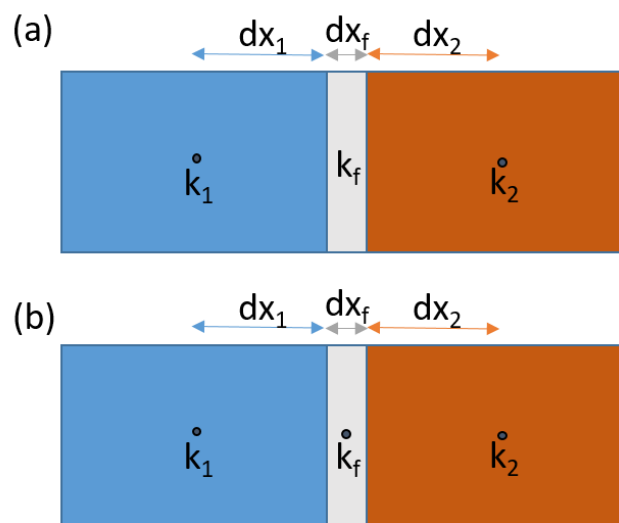


Figure 10: Example of (a) a modified conductance approach and (b) a continuum approach. The continuum approach represents the fault zone explicitly with a cell of dimension dx_f and k_f .

In this way, although the fault is not explicitly modelled, the conductance term between cells 1 and 2 is modified. The advantage of this method is that the numerical cost of implementing the horizontal effects of the flow is much lower than for explicitly modelling the fault. This approach does not account for flow within (e.g. up and along) a fault. The extent of this being a drawback is likely to depend on the scale of the problem and the properties of the fault (i.e. fault core width and permeability). This method can be easily implemented in MODFLOW-USG by correcting the inter-cell conductance between two cells separated by a fault.

4.2.2 Continuum approach

The second method for implementing the permeability modification of faults is the continuum method. Here a cell is used to explicitly represent the fault and its properties (Figure 10b). Within a regular horizontal grid this requires the addition of cells. The properties of the connection can be determined using standard inter-block calculations. The method requires the addition of one cell for every non-neighbour cell pair. The drawback of this method is that it increases the computational burden significantly. If a fault extends primarily in one direction across the model domain, the effect is similar

to increasing the discretisation in the perpendicular direction for that row of cells. The upshot however is that flow across the fault can be simulated.

5. IMPLEMENTATION OF UP-FAULT FLOW CONNECTIONS

In this section of the work we implement and investigate several methods for the inclusion of the conduit properties of faults. We specifically investigate this with an aim to implement the method to investigate the potential for propagation of depressurisation along fault planes. The flow models we discuss are presented in Figure 11.

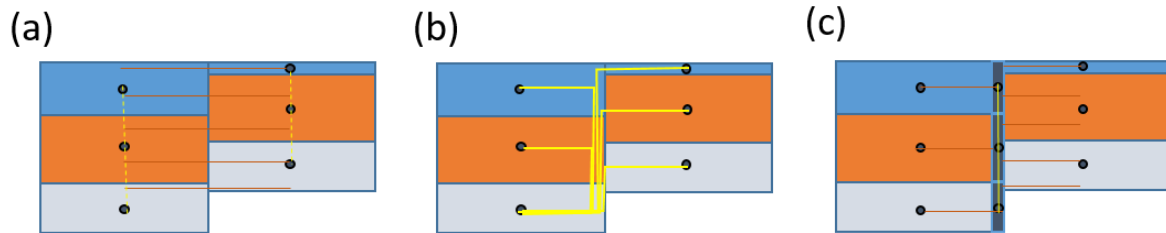


Figure 11: Conceptual model for up-fault flow implementation. (a) Modified vertical conductance (dashed yellow lines) in cells neighbouring the fault. (b) Direct connections (note only connections for the bottom left cell are shown) and (c) the continuum approach where up-fault flow occurs through a series of connected thin 'fault cells'.

5.1 Modified Conductance (Manzocchi) and vertical conductance

In this approach, the cross-fault flow is approximated with a conductance term as per the method of Manzocchi (equation 6), while the up-fault flow is presented by modifying the vertical permeability of the cells adjacent to the fault (Figure 11a). This method does allow for some up-flow mechanisms, however, it does not allow for fault flow to bypass aquitards or low flow units. It also distributes the flow over the entire area of cells. The advantage is that it utilises the existing connections within the model, effectively making the computational burden of implementation less than for explicit fault representations.

5.2 Modified Manzocchi with cross and up-fault connections

In this approach, both the cross-fault and up-fault flow are approximated with a conductance term (Figure 11b). A schematic for the calculation is presented in Figure 12. The conductance term can be given as (assuming $dx=dy$):

$$C_{12} = \frac{dx}{\frac{dx}{2K_1b_1} + \frac{dz}{K_f b_f} + \frac{dx}{2K_2b_2}} \quad (7)$$

Where C_{12} is the conductance term between the two cells, K_1 , K_2 and K_f are the hydraulic conductivities of cell 1, cell 2 and the fault and b_1 , b_2 and b_f are the thicknesses of cell 1, cell 2 and

the fault. dz is the vertical distance that water travels through the fault. To the author's knowledge, this approach has not been previously attempted.

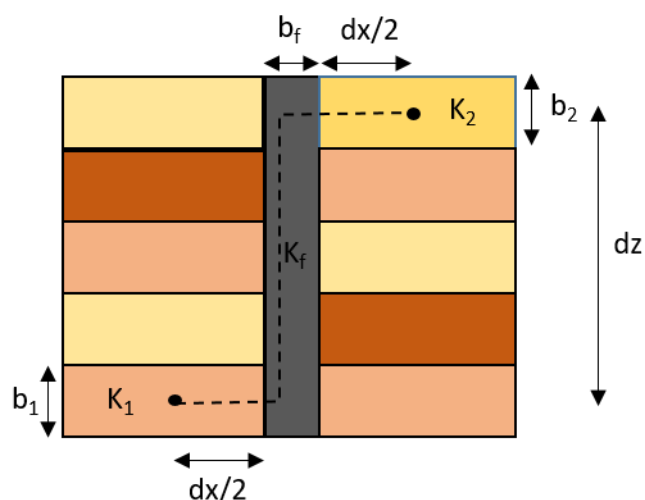


Figure 12: Schematic for the modified Manzocchi method with cross and up-fault flow connections.

This method allows for the bypass of aquitards and interburden, however the numerical cost of implementing this method in a robust manner is higher than for methods that utilise existing connections. This is because if direct connections are made between multiple layers, a large number of non-zero elements are implemented in the conductance matrix. This increases the computational burden. It also does not allow for time lags in pressure change or storage properties within the fault. In terms of implementing it in MODFLOW-USG, the large number of non-zero, off-diagonal matrix elements cannot be handled by the solver which is designed for the weakly non-symmetrical problems that arise in standard implementation.

5.3 Continuum approach.

The continuum approach, where faults are represented explicitly by actual cells, also may be used to represent up-fault flow (Figure 11c). This method has been implemented previously in other regional scale models (Celia et al., 2015; Leray et al., 2013; Magri et al., 2010; Wellmann and Croucher, 2014). The main advantages of this method are that conduit flow behaviour can be accurately represented while also allowing for horizontal bypass of less permeable layers along fault planes. The drawback is that the explicit representation of the fault or faults increases the number of cells in the model which results in a potentially significantly greater computational burden. Despite this, the connections of faults better adhere to standard numeric structures (i.e. approximately tri-diagonal) and are able to be solved with the standard solvers available in MODFLOW-USG.

6. METHOD COMPARISON

The methods presented in the previous section provide a theoretical framework for incorporating the hydraulic properties of faults in cellular groundwater models. Not all of these methods are able to be implemented in MODFLOW-USG due to the matrix structures produced, namely the modified Manzocchi method with up-fault and cross fault connections. The large number of off-diagonal elements that arise from this method are not able to be solved using the MODFLOW-USG solvers. Therefore, for the completeness of a comparison, we have implemented the method on a small model that can be solved directly in linear algebra packages like Matlab or Numpy. In this section we compare five methods for representing faults in groundwater models and subsequently simulate the effects of varying fault properties on groundwater flow using a hypothetical, small-scale three-dimensional model. The five methods tested were based on i) no conductivity modification for cells adjacent to fault location, ii) modification of horizontal conductivity terms only (Section 4.2), iii) cross fault multipliers with a vertical conductance modification (Section 5.1), iv) up- and cross-flow connection (Section 5.2) and v) the continuum approach (Sections 4.3 and 5.3). The model implemented the same equations as MODFLOW-USG.

6.1 Governing Equations

The CVFD method implements Darcy's law on a finite grid. The conductance between two connected cells i and j was calculated as:

$$C_{ij} = \frac{K_{ij} A_{ij}}{dl_{ij}} \quad (8)$$

where K_{ij} is the effective hydraulic conductivity of the connection (usually taken as the harmonic mean for cross-fault flow), A_{ij} is the effective area of the connection and dl_{ij} is the length of the connection.

For a single connection between cells i and j the system of equations is represented as:

$$\begin{bmatrix} -C_{i,j} & C_{i,j} \\ C_{i,j} & -C_{i,j} \end{bmatrix} \begin{bmatrix} h_i \\ h_j \end{bmatrix} = \begin{bmatrix} F_i \\ F_j \end{bmatrix} \quad (9)$$

where h_i and h_j are the heads in cells i and j and the F term represents sources or sinks. The equations can be summed for all connections for values of i and j between one and the number of total cells (N), resulting in an $N \times N$ matrix. The final solution of the system of equations accounting for known head values (i.e. constant head boundaries) and known fluxes (\mathbf{F}) becomes:

$$\mathbf{C}_{uu} \mathbf{h}_u = \mathbf{F}_u - \mathbf{C}_{uk} \mathbf{h}_k \quad (10)$$

where \mathbf{C}_{uu} represents a matrix of conductances between cells with unknown heads, \mathbf{h}_u and \mathbf{h}_k represent vectors of known and unknown heads, \mathbf{F}_u represents water sources to cells where the heads

are unknown and C_{uk} is the conductance between cells with unknown heads and cells with known heads. The known heads represent locations where head values have been specified.

6.2 Local-scale model implementation

The numerical model for the testing of fault implementation methods is presented in Figure 13. The model chosen was a simple three-layer system with three sets of faults (i.e. three fault faces) based on the conceptual model of Childs et al. (2009). The model represents a fault and relay zone. The model contained 7 cells in the x-direction, 12 cells in the y-direction and three cells in the z-direction. The case represents a conceptual fault zone and still includes a moderate level of complexity. The horizontal discretisation was set as 10 m and the vertical discretisation as 5 m. Constant head boundaries were set on the left and right sides of the model. On the left, the head varied linearly between 148.8 m at $y = 0$ m to 150 m at $y = 120$ m. On the right side of the model the head varied between 146.4 m at $y = 0$ m and 147 m at $y = 120$ m. These heads created a gradient perpendicular to the fault plane. The properties of the model layers are presented in Table 2.

Table 2: Fault properties used for method testing simulations. K_h is the horizontal hydraulic conductivity, and K_v is the vertical hydraulic conductivity.

Model layer	K_h (m/day)	K_v (m/day)	Thickness (m)
1	1	0.1	5
2	1.0×10^{-3}	1.0×10^{-4}	5
3	0.1	1.0×10^{-2}	5

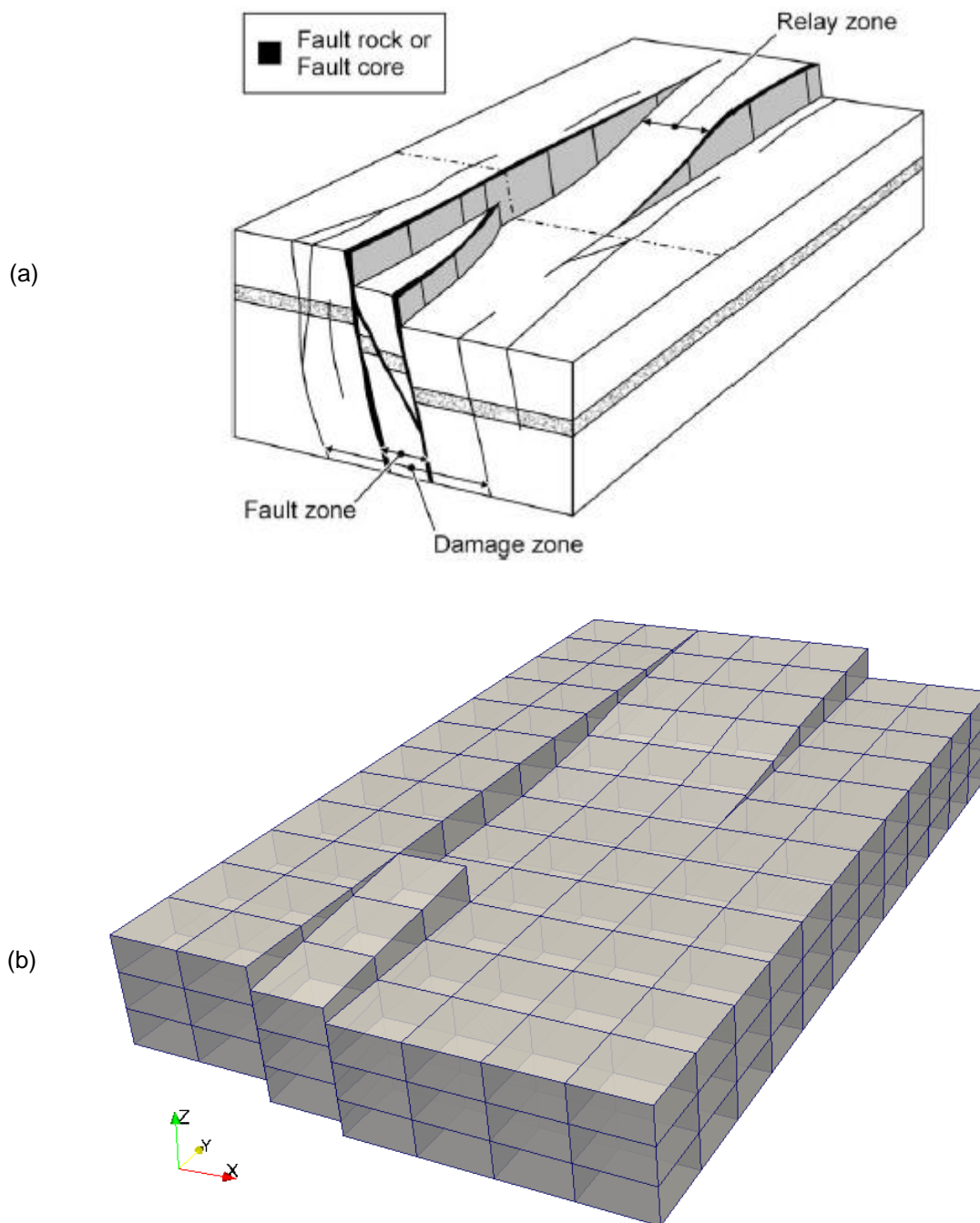


Figure 13: (a) Conceptual model (Childs et al. 2009) and (b) grid of test model. The grid is a 7 by 12 by 3 cells. The horizontal discretisation is 10 m and the vertical discretisation is 5 m. Part (a) reprinted from *Journal of Structural Geology*, Volume 31, Issue 2, C. Childs, T. Manzocchi, J. J. Walsh, C. G. Bonson, A. Nicol, M. P. J. Schöpfer, A geometric model of fault zone and fault rock thickness variations, Pages 117-127, Copyright (2009), with permission from Elsevier.

The model tested the three conceptual fault representations discussed in Section 1.3. These conceptualisations were for a fault acting as a barrier, a fault acting as a conduit and a combined conduit/barrier system. A conceptual model of the permeability of these three systems was taken from Aydin (2000, Fig. 14). The fault permeability models also required an estimate of the damage zone and fault core width (also see Figure 13). These values were taken from the relationships presented in Childs et al. (2009). A fault throw of 5 m was assumed. The values for the width of the damage zone

and fault core were taken to be 2 m and 0.05 m respectively. Childs et al. (2009) present a thorough collation of data for damage zones and fault cores. One of their key outcomes is a cumulative distribution of the ratio of displacement to thickness of fault cores and damage zones. The reader is directed here for guidance on the range of possible values for these parameters. The equivalent vertical and horizontal properties of the fault were calculated using the arithmetic and harmonic mean, respectively. The three fault scenarios tested are outlined in Table 3.

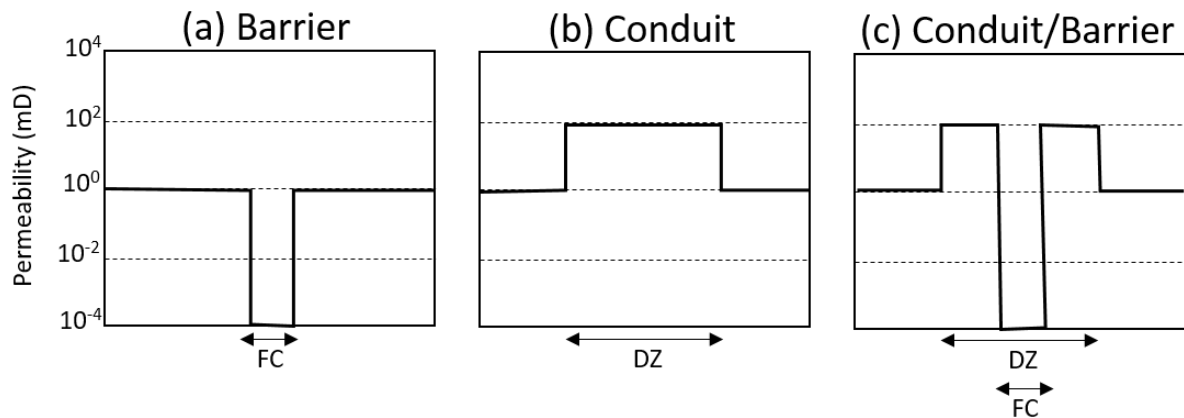


Figure 14: Permeability models of faults as (a) barrier, (b) conduit and (c) conduit/barrier systems. These conceptual models are taken from Aydin (2000). DZ represents the damage zone and FC represents the fault core. The models here are for a wall rock with a permeability of 1 mD.

Table 3: Equivalent fault flow properties for the three conceptualisations tested. K_{perp} (or K_h) and K_{par} (or K_v) represent the hydraulic conductivities perpendicular and parallel to the fault, respectively. The perpendicular properties were calculated as the harmonic mean and the parallel properties were calculated as the weighted arithmetic mean.

Model component	Scenario	Barrier	Conduit	Conduit/Barrier
Damage Zone	Width (m)	-	2	2
	k (mD)	-	100	100
	K (m/day)	-	0.83	0.83
Fault Core	Width (m)	0.05	-	0.05
	k (mD)	1×10^{-4}	-	1×10^{-4}
	K (m/day)	8.34×10^{-7}	-	8.34×10^{-7}
Equivalent Fault Properties	Width (m)	0.05	2	2
	K_{perp} (m/day)	8.34×10^{-7}	0.83	3.33×10^{-5}
	K_{par} (m/day)	8.34×10^{-7}	0.83	0.81

Five numerical fault implementations were undertaken:

- 1) Modified horizontal flow based on bisecting face fault throw (Section 4.1, Figure 6b),
- 2) Modification of the horizontal flow connections only based on the Manzocchi method for across-fault flow modification (Section 4.2.1, Figure 10a),

- 3) Accounting for across-fault flow with the Manzocchi method for cross-fault flow and accounting for up-fault flow by modifying the vertical conductance of neighbouring cells (Section 5.1, Figure 11a),
- 4) Implementing up- and across-fault flow connections directly according to the modified Manzocchi approach (Section 5.2, Figure 11b),
- 5) Using a continuum approach in which the faults are explicitly represented as cells (Section 4.2.2 and 5.3, Figure 11c).

For each of the three fault flow property conceptualisations, the total flux through the model and the heads were compared. The continuum approach was the only approach that represented the fault explicitly. This meant that both up-fault and along-fault flow were possible. We have made the assumption that this is the baseline simulation for comparison. This allowed for the absolute mean difference of the heads in all cells to be calculated for the four techniques in comparison to the continuum technique.

6.3 Results

An example simulation of the modelled system is represented in Figure 15. Although similar permutations of this figure could be shown, the head solutions are only slightly different and are therefore not included here. The depicted scenario represents the head distribution obtained for the continuum approach using the conduit-barrier conceptualisation of the fault. The influence of faults on the simulation is quite evident from the head distributions present in the vicinity of the faults.

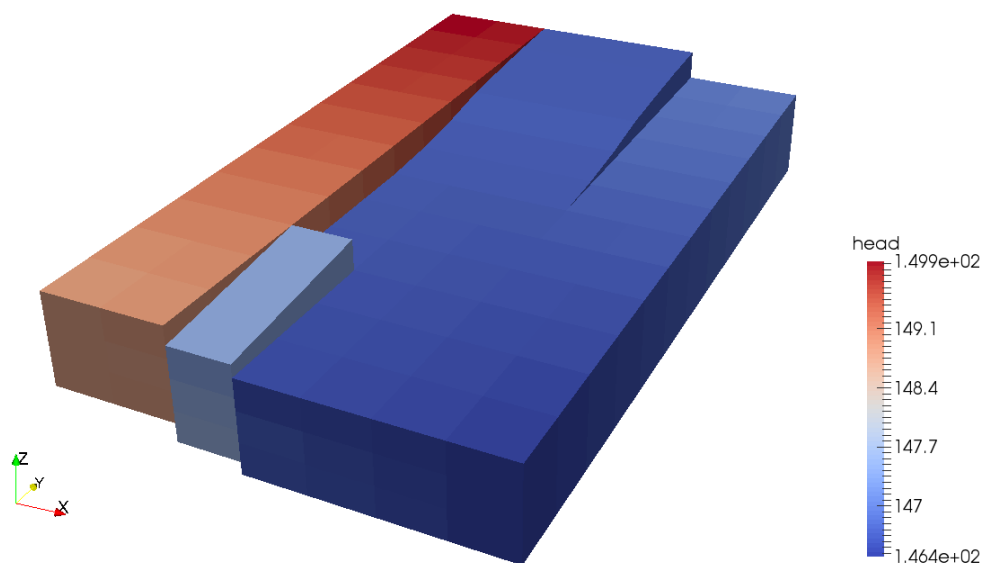


Figure 15: An example simulation using the continuum approach and the conduit/barrier conceptualisation of the fault system.

Table 4: Comparison of fault conceptualisations using calculated total flux and heads for five fault numerical methods. Flux indicates the total flux through the model in m³/day and AMD is the absolute mean difference obtained by comparing the heads of each conceptualisation with those of the continuum method.

Fault conceptualisation	Metric	Method 1: Fault throw Only	Method 2: Manzocchi	Method 3: Vertical Conductance	Method 4: Up-Fault	Method 5: Continuum
Barrier	Flux (m³/day)	14.9	0.3	0.3	0.3	0.3
	AMD (m)	12.2	0.1	0.1	0.01	-
Conduit	Flux (m³/day)	14.9	15.4	15.4	23.8	13.8
	AMD (m)	3.1	3.10	4.23	3.62	-
Barrier/ Conduit	Flux (m³/day)	14.9	15.4	15.4	0.59	11.6
	AMD (m)	2.4	2.3	2.3	9.8	-

Table 4 presents the results of the numerical comparison. The flow through the model produces an interesting comparison. When the fault is acting as a barrier to flow, the numerical methods produce similar results. All of the methods that account for fault permeability produce similar fluxes and heads. The absolute mean difference for heads is a maximum of 0.1 m with the up-fault model producing a difference of only 0.01 m. The fluxes are identical. For the case of conduit flow, methods vary in their representation of heads and flows. The largest conceptual difference between the continuum and the other methods is the potential for horizontal flow across the fault plane. This could potentially be approximated using empirical approaches by applying the same up-fault properties to the horizontal connections. Differences are also observed for the conduit barrier system. These differences are also likely due to the lateral flow along the fault plane.

Interestingly, in the case where faults act as barriers to flow, the methods provide similar results. This suggests that if a fault can be confirmed as a barrier to flow, simple implementations may be appropriate. The observed differences in conduit systems or conduit/barrier systems may be due to the somewhat two-dimensional conceptualisation of the fault flow system. For example, the conductances are generally referred to as cross- and up-fault flow. The methods could be extended to simulate along-fault flow in horizontal cells.

This comparison also represents a limitation in terms of hydrogeology and flow field complexity. For thoroughness this comparison will be extended to a wider range of aquifer, damage zone and fault core permeabilities. We will also attempt to reconcile the differences by incorporating an along flow term in an empirical approach. However, for now we will focus on the implementation of the continuum approach in a regional scale model.

7. REGIONAL SCALE MODEL IMPLEMENTATION

As the final component of our work we have applied the conceptualisation of faults to a large-scale regional model based on the faulting structure of the Gloucester Basin, New South Wales. Faults will be represented using the continuum approach. The structure of the model was based on the major faults of the Gloucester basin as previously defined in Frery et al. (2015) and Peeters et al. (2016). The position of the major faults is inferred from geological maps and geological modelling (Frery et al., 2015). In this interpretation of the structural features of the Gloucester Basin, less faults are identified compared to the ones identified on the regional geological map (Roberts et al., 1991). A 42-layer geology model was up-scaled from a local facies model of the Stratford area (Frery et al., 2015). This extended model has not been published previously and was provided to Flinders University by CSIRO.

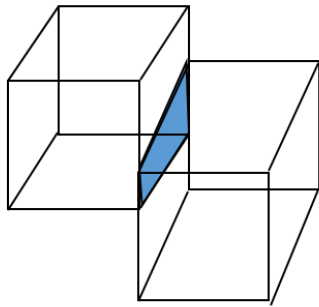
The geology model with major faults was selected in the current study to generate a realistic and generalised fault model to provide a demonstration case for the testing of idealised fault conceptualisations. To this end, no model calibration and validation were conducted using field data. However, the model can be considered a generic application for testing of fault behaviour by varying fault characteristics within reasonable and useful parameter bounds. Nevertheless, to constrain the parameter space and to ensure model behaviour was broadly representative for sedimentary coal basins in Eastern Australia, a model was developed that is based on real field data as much as possible. Under those conditions, there is no need for a strict resemblance to the field site. One limitation of the current model is that it lacks representation of sub-seismic faults. This reduces the total offset of layers. The impact of this is not clear without a comparison test. Additionally, the geology model does not consider secondary processes like cementation meaning the permeability based on the sedimentary facies of the Stratford model (Frery et al., 2015) is larger than what has been observed from core permeability estimates at the site (Parsons Brinkerhoff, 2015). Therefore, although the testing of different fault conceptualisations in models will provide a greater understanding of the role of faults on regional groundwater flow in the Gloucester Basin, the simulated flow behaviour will not necessarily correspond to site-specific behaviour because of the limitations highlighted above. The advantage of the use of a generalised fault model and fault parameters is that its results have greater transferability to other basins.

7.1 Model Description

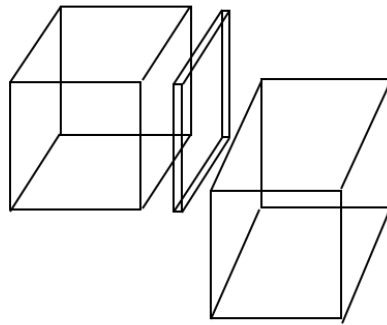
Implementation of the continuum approach to fault simulation methodology in the geology model involved the following steps which are also demonstrated in Figure 16:

- 1) Identify non-neighbour connections existing at each of the faults (Fig. 16a),
- 2) Determine if a fault node already existed for this point,
- 3) If no fault node existed, copy the face of the lower node and connect the lower geology model node to the fault (Fig 16b),
- 4) Calculate the connection properties of the opposite node (Fig 16c),
- 5) Connect the fault nodes to adjacent fault nodes (Fig. 16d), and
- 6) Implement ghost node corrections for the faulted faces (see Section 3.3).

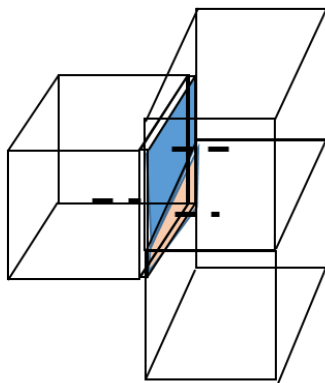
(a) Connected cell area



(b) Create fault node



(c) Connected cells to fault cell



(d) Connected to adjacent fault cells

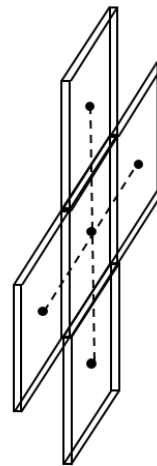


Figure 16: Implementation of the continuum method in MODFLOW Unstructured grid

One of the main objectives of this exercise was to simulate the effects of varying fault behaviours on both deeper and shallow groundwater. For this reason, a shallow alluvial aquifer including several streams was integrated in the regional-scale model. The alluvial aquifer extent was based on a shape file of the alluvium in the Gloucester basin. A spatially uniform hydraulic conductivity of 5 m/day was selected to be within the range of values reported for the alluvial aquifer sediments by Peeters et al. (2016). The process of integrating the alluvial model into the regional one involved the connection of the alluvial aquifer cells to the underlying and adjacent structural geology model. The model also implemented a quad-tree refinement, where the extent of the cells was one third of that of the underlying aquifer. Boundary conditions for the alluvial aquifer were selected to be similar to those presented by AGL Energy Limited (2015). The model implemented a drain package to simulate the streams in the area as a discharge feature; a recharge rate of 80 mm/year was used for the alluvial aquifer and 2.5 mm/year for the fractured rock aquifer. No evapotranspiration was simulated. To stress the model according to the projected coal seam gas development (now abandoned and thus no longer a current but purely hypothetical projection), coal seam gas wells were added to model layer 22. This represented pumping from a target seam. A maximum pumping rate of 12 m³/day per well was distributed over a 1 by 2 km area using 50 pumping wells for 1 year, the rate then declined (exponentially) to zero over a period of 23 years. The pumping history was based on the P50 Scenario from AGL Energy Limited (2015). This represented the median pumping scenario for the coal seam gas extraction. The model

grid is presented in Figure 17. Figure 17a presents a plan view of the model where the implementation of the refined alluvial model is observed. Figure 17b shows the distortion of the vertical layering due to faulting and Figure 17c presents the horizontal hydraulic conductivity (geometric mean of the aquifer hydraulic conductivity = 0.43 m/day).

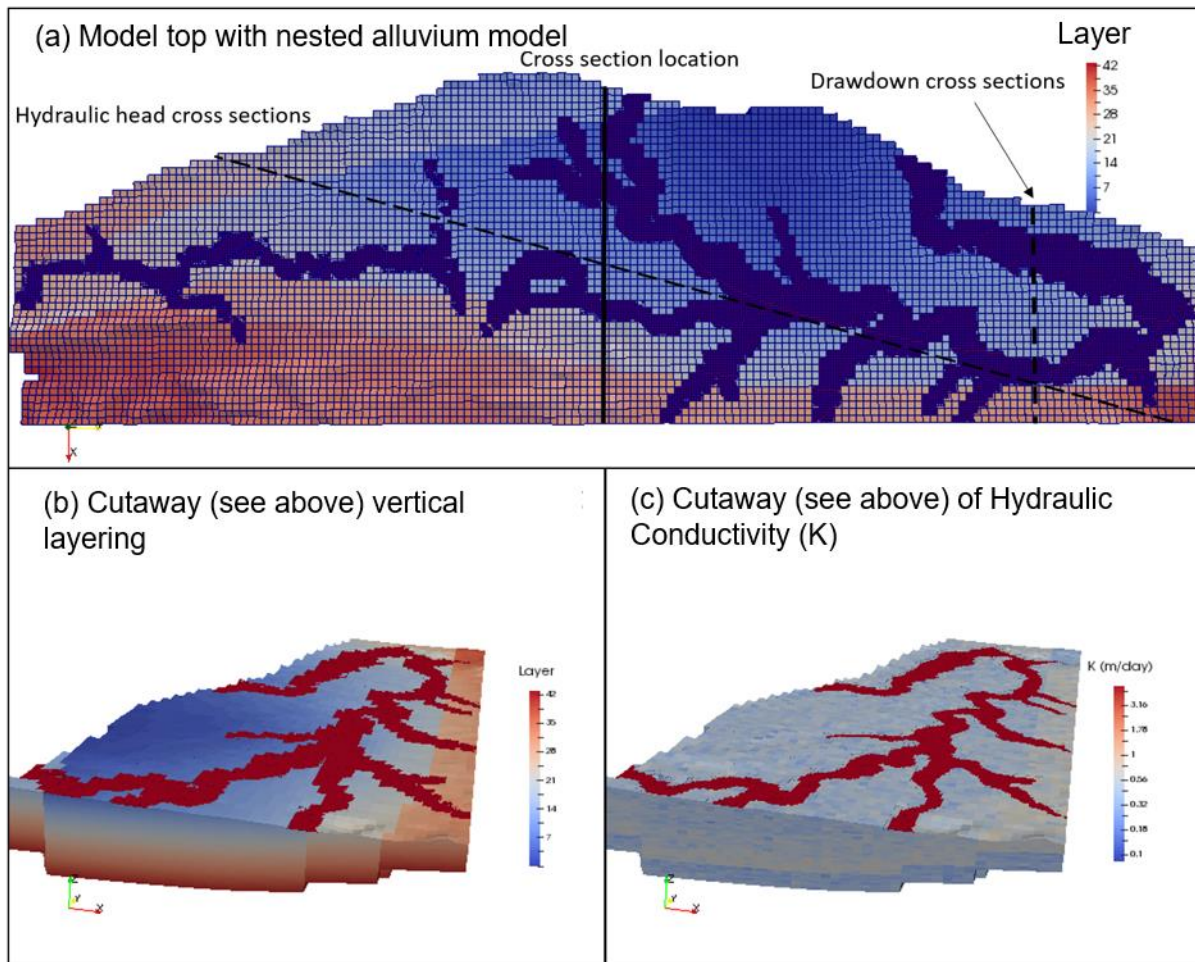


Figure 17: Model setup with (a) plan view with layer numbers (variability in layer numbers at the surface is due to fault juxtaposition), (b) cross section view of model domain (showing discontinuities created by faulting), and (c) Hydraulic conductivity distribution. Part (a) also shows the location of the cross sections used for head and drawdown results.

The regional model was tested for the three fault conceptualisations identified from the literature review (see section 1.3). These conceptual models define faults as behaving as conduits, barriers or conduit barrier systems. Table 5 outlines the properties used for each of the models. Thicknesses of the fault core and damage zone were estimated from the plots presented in Childs et al. (2009) and assuming a uniform fault displacement of 300m. This was achieved by using Figures 4a and 4f (Childs et al., 2009) and selecting a value consistent with a throw of 300m.

Table 5: Fault properties for the scenarios tested in the regional model. Thicknesses based on the relationships presented in Childs et al. (2009) and assuming a uniform 300m fault displacement and permeabilities based on the conceptual models of Aydin (2000). Across fault flow (K_h) is taken as the harmonic mean and the up fault flow (K_v) is taken as the arithmetic mean (see Table 3 for terminology and calculation example).

	Scenario	Barrier	Conduit	Conduit-Barrier
Damage Zone	Width (m)	-	10	10
	k (mD)	-	100	100
	K (m/day)	-	0.83	0.83
Fault Core	Width (m)	1	-	1
	k (mD)	1.0×10^{-4}	-	1.0×10^{-4}
	K (m/day)	8.34×10^{-7}	-	8.34×10^{-7}
Bulk Fault Properties	Width (m)	1	10	10
	K_h (m/day)	8.34×10^{-7}	0.83	8.34×10^{-6}
	K_v (m/day)	8.34×10^{-7}	0.83	0.75

Overall, this model resulted in a large number of cells, consisting of 166,522 model cells. This included 144,666 regional geology cells, 7,516 fault cells, and 14,377 alluvial model cells. The model also implemented 11,496 ghost node connections for fault cells and 14,273 ghost node connections to nest the alluvial model. This is a large model, however for the 200 year transient simulations with an initial steady-state time step the runtimes were of the order of 12 minutes. This suggests that the overall approach is still efficient despite the large number of additional connections and the complexity of the model.

7.2 Results

Figure 18 represents the steady-state hydraulic heads from the initial steady-state simulations. In Figures 18a and 18c step changes in the head solution are observed at faults. Both of these methods implement a horizontal barrier to flow. In the case where the fault is implemented as a high permeability conduit (Fig. 18b), the heads vary smoothly around the faults. This is consistent with the concept that the faults do not act as barriers to flow. The ability to observe a gradient at a fault will depend on the density of observation points near the well. For example, if wells are located across a fault at large distances, it may be difficult to distinguish if the gradient is a step change or smooth change.

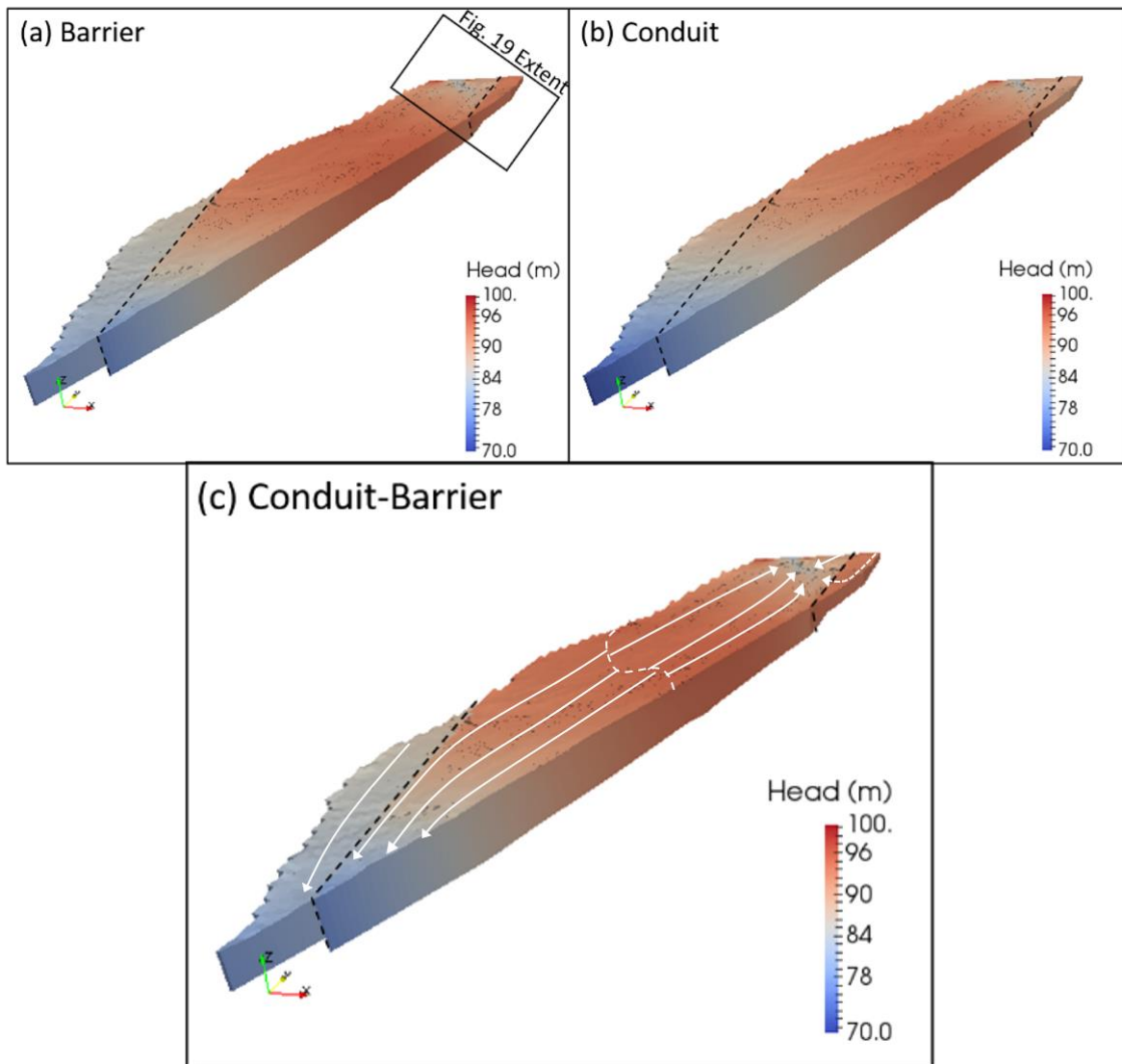


Figure 18: Initial head distributions for the three fault conceptualisations. The fault locations are represented by the dashed black lines. The location of the transect line is shown in Figure 17. (c) shows the general flow direction in the system, the dashed white line represents a flow division in the centre of the model. Flow across the faults (dashed white arrow in the right on the model) will depend on the fault type and characteristics.

Given the relatively short duration of the maximum pumping rate (12 m³/day from each of 50 wells for 1 year) in this investigation, it is unlikely that the system will have reached steady state conditions. Nevertheless, maximum drawdown is reached after 365 days of pumping inducing the greatest impact on the groundwater flow. Comparison of the groundwater drawdown and head prior to, and 365 days after pumping will reveal the effect of the different fault types on the groundwater flow system under a realistic pumping scenario.

Figure 19 represents the areas of drawdown 365 days after pumping commenced, where the fault is located at the left face of these plots. The observable differences in these plots is the extent of the drawdown along the fault. The impact of the fault is most notable in Figure 19a and 19c, which show that the drawdown stops sharply at the fault. In Figure 19b, the drawdown is observed to extend beyond the fault. Closer examination of the conduit-barrier conceptualisation (Figure 19c) shows a greater

extent of intermediate drawdowns extending along the fault face when compared to Figure 19a. The interesting outcome is that in scenarios (a) and (c) the drawdown beyond the fault is much less owing to the resistance to flow exerted by the fault (barrier and conduit-barrier case). This suggests that the characterisation of the fault properties will have an important impact on the flow predictions made.

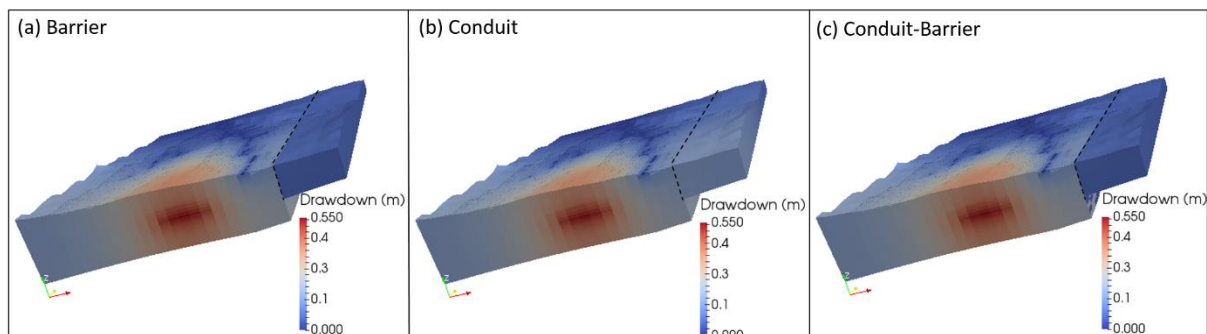


Figure 19: Drawdowns after 365 days. The location of the transect line is shown in Figure 17. The fault location is represented by the dashed line.

Figure 20 represents an east-west cross section (perpendicular to the fault) of the drawdown cone from the pumping scenario described in section 7.1. The drawdowns are aggregated across all layers due to the faulting and the non-uniform subsurface grids not allowing layer based plots. The two methods that restrict horizontal flows (barrier and conduit/barrier conceptualisations) display almost exactly the same drawdown pattern. The location of the fault is evident in the plots due to the sharp change in drawdowns. East of the fault, drawdowns are significantly lower than on the west of the fault. For the conduit scenario, the drawdown extends beyond the fault. An inflection point occurs in the area of the fault. Although the fault is not acting as a barrier, the uplift has reduced the transmissivity on the eastern side of the fault. The reduction in transmissivity impacts the extent of the drawdown.

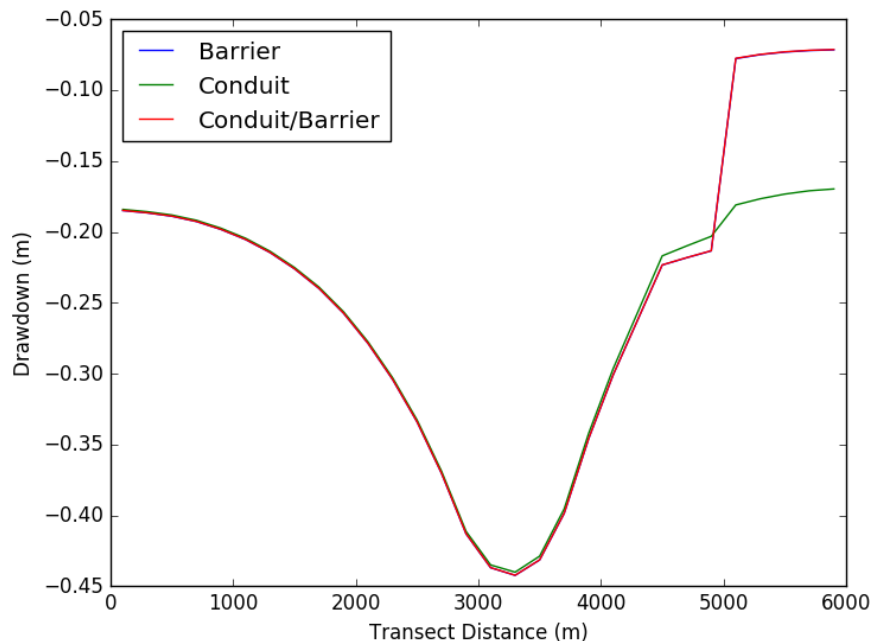


Figure 20: Layer-averaged drawdown along East-West transect (orthogonal to the faults) as shown in Figure 17(a). The fault is located at 5000 m. (Barrier and Conduit/Barrier are essentially identical)

The vertical head distribution at both sides of a fault will alter depending on the fault type and its properties relative to the background permeability. This may have an impact on the broader head distribution (vertical and horizontal) in the adjacent aquifers. The effect on the head distribution will be determined by the flux across the fault. Conduit faults will have limited effects on the flow and vertical gradients when their hydraulic conductivity is similar to the background hydraulic conductivity. As will be shown next, the effects of barrier faults on horizontal gradients and flow may be significant; the effect on vertical head distribution will be shown to be rather small. Figure 21 represents the vertical head distribution at three locations (within the drawdown cone, east of the fault and west of the fault) along the transect shown in Figure 17; the vertical head distributions are compared before pumping and 365 days after pumping has commenced.

To the east of the fault (Figure 21(d)), and for all three fault conceptualisations, there is little to no change in hydraulic head with depth owing to existence of a single layer with relatively uniform K distribution. Modelling results to the west of the pumping field (Figure 21(b)) show a persistent downward gradient (head values decrease with depth), primarily driven by surface recharge.

For the conduit fault (at both $t = 0$ and $t = 365$ days), the heads in Figure 21(c) are lower in the top 600 m compared to the bottom 400m. This is the result of a higher hydraulic conductivity in the top 600 m, while the bottom 400 m is less permeable resulting in a small pressure (head) build-up. The specific and non-uniform vertical head distribution is likely the combined effect of aquifer geometry/transmissivity, overlying alluvial sequence (area of high recharge) and adjacent boundary conditions (fault and no flow where the deepest layer stops along the bottom half of the fault). The area adjacent and east to the fault exhibits Tóthian nested flow systems, whereby the alluvial sediments (and drains within the alluvium) create local flow systems that sit within the deeper reservoir flow system (Figure 22).

In the case of the barrier and conduit/barrier conceptualisations, the fault acts as a low flow boundary, resulting in a head drop of nearly 3 m across the fault (compare heads immediately east and west of the fault, Figure 21c-d). In the case of the conduit fault, the head drop across the fault is very small, on the order of several centimetres.

Interestingly at all locations and in all cases, pumping does not modify the shape of the vertical head distribution. Rather, the head distribution shows lower values due to the drawdown, albeit very limited close to the fault. The role of the barrier fault may become more apparent when higher pumping rates are applied. This indicates that the hydraulic head differences are propagated through the model uniformly within a simulation time frame of 365 days. This is likely due to the high values of hydraulic conductivity within the model (0.1 – 1.0 m/day).

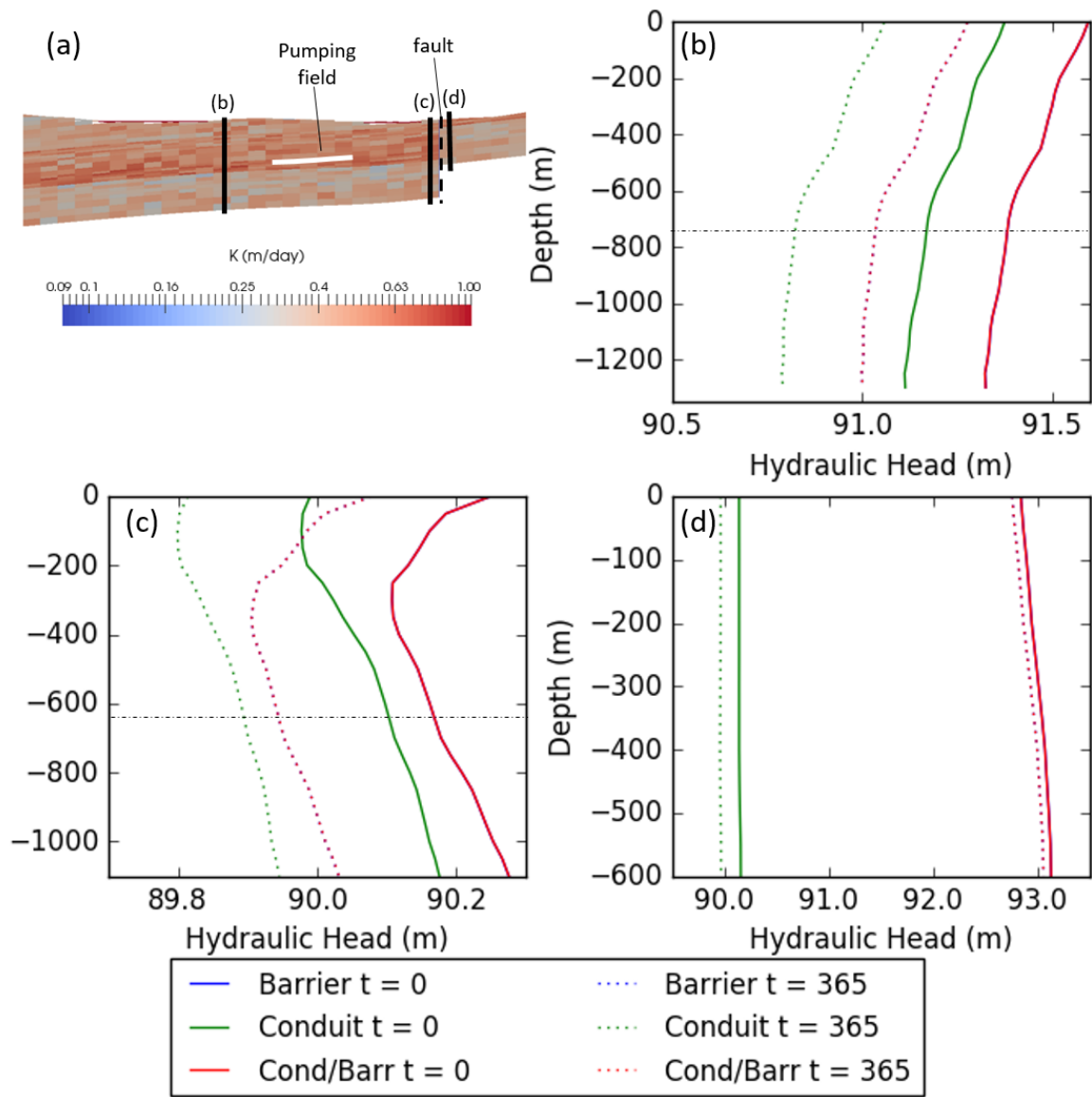


Figure 21: Vertical head distributions for different fault flow conceptualisations prior to pumping ($t = 0$ days) and after 365 days of pumping ($t = 365$ days) at different positions along a cross section shown in (a). (a) shows the cross section from which the vertical gradients (labelled b, c, and d) were taken, the location of this transect is shown in Figure 17 labelled as 'Drawdown cross section'. (b) shows the vertical gradient within 400 m west of the pumping field (see (a) for location), (c) shows the vertical gradient 95 m west of the fault and (d) shows the vertical gradient 95 m east of the fault. The dashed horizontal line in (b) and (c) indicates the transition from a higher hydraulic conductivity zone to a lower hydraulic conductivity zone. (Barrier and Conduit/Barrier are identical).

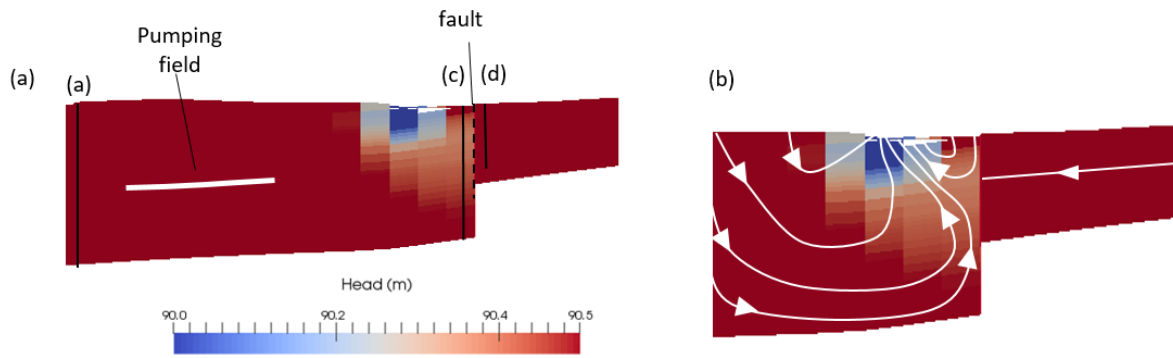


Figure 22: (a) Example of the hydraulic head distribution, prior to pumping ($t = 0$ days), for the barrier fault conceptualisation. (b) A schematic diagram of the flow lines (white lines) for the cross section (barrier fault and $t = 0$ days). With a barrier fault, there is nearly no flow across the fault; east of the fault, flowlines close to the fault will be predominantly along the fault.

8. DISCUSSION

In this study we have discussed three conceptualisations of fault behaviour and investigated techniques to represent them in numerical models for regional groundwater applications. The conceptualisations of fluid flow associated with faults can be summarised as barriers to flow, conduits to flow and combined conduit-barrier behaviour (Aydin, 2000; Caine et al., 1996; Rawling et al., 2001). The behaviour of the fault will be dependent on the relative proportions of low permeability fault core, and higher permeability damage zone (in consolidated sediments) or mixed zone (in unconsolidated sediments). Our numerical modelling has demonstrated that these three different fault conceptualisations impact the predictions made with groundwater flow models.

Our work suggests that a key aspect of model conceptualisation and parameterisation is the characterisation of fault behaviour. Ideally, field programs and data collection should focus on informing which of these behaviours should be implemented in regional models. However, if this conceptualisation and parameterisation is not possible, it may be necessary to test each of these possibilities in a sensitivity analysis or calibration exercise. This may be particularly important in determining the likely extent of drawdowns, as barrier behaviour is likely to restrict the area impacted by drawdown. In the case presented here, drawdown close to the pumping well was not affected by these fault barriers. However, it is likely that in some environments, horizontal restriction may increase local drawdowns, especially if the fault is in close proximity to the pumping well. In our case, the pumping well is sufficiently far away for the drawdown not to be impacted by the fault. Whether or not the fault has a significant effect on local drawdown will depend on pumping rates, aquifer properties, fault properties, and time to drawdown observation.

Whilst the fault core permeability can be determined by methods like the shale gouge ratio (Bense and Person, 2006; Childs et al., 2007; Manzocchi et al., 1999), one of the greatest difficulties with the proposed conceptualisations is the characterisation of the damage zone. Although the initial process of faulting will lead to fracturing, secondary processes like cementation and changes in the regional stress field may reduce fracture apertures and permeabilities. The only existing model that captures the strong anisotropic structures within the fault core was developed for unconsolidated sediment and hence is not representative of the environments that this project is focussed on (Bense and Person, 2006). It may be harder to develop generic models of the damage zone permeabilities for fractured rocks. Additionally, Childs et al., (2009) suggested the damage zone width was the most difficult to characterise from fault displacement data.

In our current example we have only simulated a limited set of examples. The behaviour of faults will be dependent on a number of factors including the permeability distribution of the system, the geometry of the basin, the recharge and discharge characteristics of the basin and the stresses placed on the system. We plan to extend this work to a greater range of scenarios to improve the generality of our results.

The ability of the different methodologies to simulate flow behaviour is dependent on the fault conceptualisation (e.g. conduit, barrier, or conduit/barrier). In general, the methods give similar results for faults that are barriers, however between conduit and conduit/barrier hybrids there is less

agreement. The difference appears to relate to the potential for horizontal flow across the fault plane. The methods tested in this report represent across and up-fault flow, however they do not consider along fault flow (in the third dimension). One existing methods for along fault flow simulation was proposed by Bense and Person (2006). The method proposed was for unconsolidated systems and the mechanism for permeability enhancement was the vertical alignment of layers during faulting. In consolidated sediments, the process of fracturing will also lead to along-fault flow. This mechanism could be implemented the same way as up-fault flow. Future work should consider this type of implementation.

9. SUMMARY OF PROGRESS

In this report we have outlined and tested a methodology for implementing fault properties into regional groundwater flow models. By comparing several fault implementation approaches within a systematic and quantitative framework, we have found the following:

- 1) The three fault conceptualisations (barrier, conduit and combined conduit barrier systems) result in differences in how groundwater flow behaves around faults
- 2) MODFLOW Unstructured-grid (MODFLOW-USG) offers the flexibility to represent grid geometries that arise from faulting.
- 3) We have developed a method to explicitly represent fault zones in MODFLOW-USG.
- 4) We have shown that this method can be implemented on large complex grids and converge for the three conceptual models identified.

This application of MODFLOW-USG will allow for complex and spatially variable fault geometries, permeabilities and thicknesses to be incorporated into regional flow models. It offers a numerically viable option for including faults in models. It will also allow the incorporation of complex geology models (including faults) in regional groundwater flow models.

To improve the quality of this work and the generality of the conclusions the following are still required:

- 1) An improved conceptualisation of the Gloucester basin fault system, and validation of the modelling approach using field data
- 2) Some generic modelling of a wider range of systems expected in CSG regions in Australia
- 3) A detailed sensitivity analysis of the relationships between the key damage and fault core properties that determine conduit or barrier behaviour.

10. REFERENCES

- AGL Energy Limited (2015) Gloucester Gas Project – extracted water management strategy (final 2036 draft). AGL Energy Limited, Sydney. Viewed 21 December 2015, https://www.agl.com.au/~media/AGL/About%20AGL/Documents/How%20We%20Source%20Energy/Gloucester%20Document%20Repository/Water%20Plans/20150904_GGP%20%20%200Extracted%20Water%20Management%20Strategy%20%20%20Final%20Draft.pdf.
- Allan, U.S., 1989. Model for Hydrocarbon Migration and Entrapment Within Faulted Structures. *Am. Assoc. Pet. Geol. Bull.* 73, 803–811.
- Aydin, A., 2000. Fractures, faults, and hydrocarbon entrapment, migration and flow. *Mar. Pet. Geol.* 17, 797–814. doi:10.1016/S0264-8172(00)00020-9
- Balsamo, F., Storti, F., Salvini, F., Silva, A.T., Lima, C.C., 2010. Structural and petrophysical evolution of extensional fault zones in low-porosity, poorly lithified sandstones of the Barreiras Formation, NE Brazil. *J. Struct. Geol.* 32, 1806–1826. doi:10.1016/j.jsg.2009.10.010
- Basquet, R., Jeannin, L., Lange, A., Bourbiaux, B., Sarda, S., 2003. Gas Flow Simulation in Discrete Fracture Network Models, in: *SPE Reservoir Simulation Symposium*. Society of Petroleum Engineers. doi:10.2118/79708-MS
- Benedicto, A., Plagnes, V., Vergely, P., Flotte, N., Schultz, R.A., 2008. Fault and fluid interaction in a rifted margin: integrated study of calcite-sealed fault-related structures (southern Corinth margin). *Geol. Soc. London, Spec. Publ.* 299, 257–275. doi:10.1144/SP299.16
- Bense, V.F., Gleeson, T., Loveless, S.E., Bour, O., Scibek, J., 2013. Fault zone hydrogeology. *Earth-Science Rev.* 127, 171–192. doi:10.1016/j.earscirev.2013.09.008
- Bense, V.F., Person, M.A., 2006. Faults as conduit-barrier systems to fluid flow in siliciclastic sedimentary aquifers. *Water Resour. Res.* 42, n/a–n/a. doi:10.1029/2005WR004480
- Bense, V.F., Van den Berg, E.H., Van Balen, R.T., 2003. Deformation mechanisms and hydraulic properties of fault zones in unconsolidated sediments; the Roer Valley Rift System, The Netherlands. *Hydrogeol. J.* 11, 319–332. doi:10.1007/s10040-003-0262-8
- Bour, O., Davy, P., 1997. Connectivity of random fault networks following a power law fault length distribution. *Water Resour. Res.* 33, 1567–1583. doi:10.1029/96WR00433
- Caine, J.S., Bruhn, R.L., Forster, C.B., 2010. Internal structure, fault rocks, and inferences regarding deformation, fluid flow, and mineralization in the seismogenic Stillwater normal fault, Dixie Valley, Nevada. *J. Struct. Geol.* 32, 1576–1589. doi:10.1016/j.jsg.2010.03.004
- Caine, J.S., Evans, J.P., Forster, C.B., 1996. Fault zone architecture and permeability structure. *Geology* 24, 1025. doi:10.1130/0091-7613(1996)024<1025:FZAAPS>2.3.CO;2
- Celia, M.A., Bachu, S., Nordbotten, J.M., Bandilla, K.W., 2015. Status of CO₂ storage in deep saline aquifers with emphasis on modeling approaches and practical simulations. *Water Resour. Res.* 51, 6846–6892. doi:10.1002/2015WR017609
- Childs, C., Manzocchi, T., Walsh, J.J., Bonson, C.G., Nicol, A., Schöpfer, M.P.J., 2009. A geometric model of fault zone and fault rock thickness variations. *J. Struct. Geol.* 31, 117–127. doi:10.1016/j.jsg.2008.08.009
- Childs, C., Walsh, J.J., Manzocchi, T., Strand, J., Nicol, A., Tomasso, M., Schopfer, M.P.J., Aplin, A.C., 2007. Definition of a fault permeability predictor from outcrop studies of a faulted turbidite sequence, Taranaki, New Zealand. *Geol. Soc. London, Spec. Publ.* 292, 235–258. doi:10.1144/SP292.14
- Dershowitz, W., Lee, G., Geier, J., Foxford, T., LaPointe, P., Thomas, A., 1999. User documentation for FracMan.
- Dickinson, J.E., James, S.C., Mehl, S., Hill, M.C., Leake, S.A., Zvoloski, G.A., Faunt, C.C., Eddebarh, A.-A., 2007. A new ghost-node method for linking different models and initial investigations of heterogeneity and nonmatching grids. *Adv. Water Resour.* 30, 1722–1736. doi:10.1016/j.advwatres.2007.01.004

- Du Bernard, X., Eichhubl, P., Aydin, A., 2002. Dilation bands: A new form of localized failure in granular media. *Geophys. Res. Lett.* 29, 29–1–29–4. doi:10.1029/2002GL015966
- Edwards, M.G., 1996. Elimination of Adaptive Grid Interface Errors in the Discrete Cell Centered Pressure Equation. *J. Comput. Phys.* 126, 356–372. doi:10.1006/jcph.1996.0143
- Eichhubl, P., Davatzes, N.C., Becker, S.P., 2009. Structural and diagenetic control of fluid migration and cementation along the Moab fault, Utah. *Am. Assoc. Pet. Geol. Bull.* 93, 653–681. doi:10.1306/02180908080
- Exner, U., Grasemann, B., 2010. Deformation bands in gravels: displacement gradients and heterogeneous strain. *J. Geol. Soc. London.* 167, 905–913. doi:10.1144/0016-76492009-076
- Fairley, J.P., 2009. Modeling fluid flow in a heterogeneous, fault-controlled hydrothermal system. *Geofluids* 9, 153–166. doi:10.1111/j.1468-8123.2008.00236.x
- Frery, E., H, R.-O., PG, W., TR, M., TG, V.N., LT, L., OV, B., PK, R., YQ, Z., WR, D., SP, M., H, B., MP, G., 2015. Observations analysis and statistical analysis and interpolation for the Gloucester subregion. Product 2.1-2.2 for the Gloucester subregion from the Northern Sydney Basin Bioregional Assessment. Australia.
- Gibson, R.G., 1998. Physical character and fluid-flow properties of sandstone-derived fault zones. *Geol. Soc. London, Spec. Publ.* 127, 83–97. doi:10.1144/GSL.SP.1998.127.01.07
- Gillespie, P. a., Howard, C.B., Walsh, J.J., Watterson, J., 1993. Measurement and characterisation of spatial distributions of fractures. *Tectonophysics* 226, 113–141. doi:10.1016/0040-1951(93)90114-Y
- Herbert, A.W., 1996. Modelling approaches for discrete fracture network flow analysis, in: Stephansson, O., Jing, L., Tsang, C.- F. . (Eds.), *Coupled Thermo-Hydro-Mechanical Processes of Fractured Media*. Elsevier, New York, NY, USA, pp. 213–229.
- Heynekamp, M.R., Goodwin, L.B., Mozley, P.S., Haneberg, W.C., 1999. Controls on fault-zone architecture in poorly lithified sediments, Rio Grande Rift, New Mexico: Implications for fault-zone permeability and fluid flow. *American Geophysical Union*, pp. 27–49. doi:10.1029/GM113p0027
- Kim, J.-G., Deo, M.D., 2000. Finite element, discrete-fracture model for multiphase flow in porous media. *AIChE J.* 46, 1120–1130. doi:10.1002/aic.690460604
- Leray, S., de Dreuzy, J.-R., Bour, O., Bresciani, E., 2013. Numerical modeling of the productivity of vertical to shallowly dipping fractured zones in crystalline rocks. *J. Hydrol.* 481, 64–75. doi:10.1016/j.jhydrol.2012.12.014
- Long, J.C.S., Remer, J.S., Wilson, C.R., Witherspoon, P.A., 1982. Porous media equivalents for networks of discontinuous fractures. *Water Resour. Res.* 18, 645–658. doi:10.1029/WR018i003p00645
- Loveless, S., Bense, V., Turner, J., 2011. Fault architecture and deformation processes within poorly lithified rift sediments, Central Greece. *J. Struct. Geol.* 33, 1554–1568. doi:10.1016/j.jsg.2011.09.008
- Magri, F., Akar, T., Gemici, U., A., P., 2010. Deep geothermal groundwater flow in the Seferihisar-Balçova area, Turkey: results from transient numerical simulations of coupled fluid flow and heat transport processes. *Geofluids* 10, 388–405. doi:10.1111/j.1468-8123.2009.00267.x
- Manzocchi, T., Walsh, J.J., Nell, P., Yielding, G., 1999. Fault transmissibility multipliers for flow simulation models. *Pet. Geosci.* 5, 53–63. doi:10.1144/petgeo.5.1.53
- Manzochhi, T., Childs, C., Walsh, J.J., 2010. Faults and fault properties in hydrocarbon flow models. *Geofluids* 10, 94–113. doi:10.1111/j.1468-8123.2010.00283.x
- Martel, S., 1990. Formation of compound strike-slip fault zones, Mount Abbot quadrangle, California. *J. Struct. Geol.* 12, 869–882. doi:10.1016/0191-8141(90)90060-C
- Matthäi, S.K., Roberts, S.G., 1996. The influence of fault permeability on single-phase fluid flow near fault-sand intersections: Results from steady-state high-resolution models of pressure-driven fluid flow. *Am. Assoc. Pet. Geol. Bull.* 80, 1763–1779. doi:10.1306/64EDA15E-1724-11D7-8645000102C1865D

- Panday, S., Langevin, C.D., Niswonger, R.G., Ibaraki, M., Hughes, J.D., 2013. MODFLOW-USG Version 1: An Unstructured Grid Version of MODFLOW for Simulating Flow and Tightly Coupled Processes Using a Control Volume Finite-Difference Formulation. Reston, Virginia.
- Parsons Brinkerhoff, 2015. Updated conceptual hydrogeological model of the Gloucester Basin. Sydney, Australia.
- Peeters, L.J.M., Dawes, W.R., Rachakonda, P.R., Pagendam, D.E., Singh, R.M., Pickett, T.W., Frery, E., Marvanek, S.P., McVicar, T.R., 2016. Groundwater numerical modelling for the Gloucester subregion: Product 2.6.2 for the Gloucester subregion from the Northern Sydney Basin Bioregional Assessment.
- Rawling, G.C., Goodwin, L.B., 2006. Structural record of the mechanical evolution of mixed zones in faulted poorly lithified sediments, Rio Grande rift, New Mexico, USA. *J. Struct. Geol.* 28, 1623–1639. doi:10.1016/j.jsg.2006.06.008
- Rawling, G.C., Goodwin, L.B., Wilson, J.L., 2001. Internal architecture, permeability structure, and hydrologic significance of contrasting fault-zone types. *Geology* 29, 43. doi:10.1130/0091-7613(2001)029<0043:IAPSAH>2.0.CO;2
- Roberts, G., Stewart, I., 1994. Uplift, deformation and fluid involvement within an active normal fault zone in the Gulf of Corinth, Greece. *J. Geol. Soc. London.* 151, 531–541. doi:10.1144/gsjgs.151.3.0531
- Roberts, J., Engel, B., Chapman, J., 1991. Geology of the Camberwell, Dungog and Bulahdelah 1:100,000 Sheets 9133, 9233, 9333. 382 pp. New South Wales Geological Survey, Sydney.
- Schulz, S.E., Evans, J.P., 2000. Mesoscopic structure of the Punchbowl Fault, Southern California and the geologic and geophysical structure of active strike-slip faults. *J. Struct. Geol.* 22, 913–930. doi:10.1016/S0191-8141(00)00019-5
- Sigda, J.M., Goodwin, L.B., Mozley, P.S., Wilson, J.L., 1999. Permeability alteration in small-displacement faults in poorly lithified sediments: Rio Grande Rift, Central New Mexico. *American Geophysical Union*, pp. 51–68. doi:10.1029/GM113p0051
- Sigda, J.M., Wilson, J.L., 2003. Are faults preferential flow paths through semiarid and arid vadose zones? *Water Resour. Res.* 39, n/a–n/a. doi:10.1029/2002WR001406
- Turnadge, C., Mallants, D., Peeters, L., 2018. Overview of aquitard and geological fault simulation approaches in regional scale assessments of coal seam gas extraction. Canberra, Australia.
- Underschultz, J., Esterle, J., Strand, J., Hayes, S., 2018. Conceptual representation of fluid flow conditions associated with faults in sedimentary basins. Brisbane, Australia.
- Walsh, J.J., Watterson, J., 1988. Analysis of relationship between displacement and dimensions of faults. *J. Struct. Geol.* 10, 239–247.
- Wellmann, J.F., Croucher, A., 2014. Integrating structural geological data into the inverse modelling framework of iTOUGH2. *Comput. Geosci.* 65, 95–109. doi:10.1016/j.cageo.2013.10.014
- Wilson, J.E., Goodwin, L.B., Lewis, C.J., 2003. Deformation bands in nonwelded ignimbrites: Petrophysical controls on fault-zone deformation and evidence of preferential fluid flow. *Geology* 31, 837. doi:10.1130/G19667R.1